CZECH TECHNICAL UNIVERSITY IN PRAGUE

Faculty of Mechanical Engineering

Department of Automotive, Combustion Engine and Railway Engineering

Study program: Master of Automotive Engineering

GASEOUS FUEL SUPPLY FOR A GAS ENGINE WITH A SCAVENGED PRE-CHAMBER

Author : Nishanth Nithyanandham

Supervisor : Ing. Jiří Vávra, Ph.D.

Tutor : Ing. Zbyněk Syrovátka

Year : 2018

Disclaimer

I hereby declare that this thesis work is my independent work and I have used only the documents listed in the attachments. It contains no materials previously published or written by another person.

In Prague: 20. 08. 2018

_____

Nishanth Nithyanandham

Acknowledgment

First, I would like to express my gratitude to my main supervisor Ing. Jiří Vávra, PhD. for all the guidance, support and patience throughout my master thesis. I am equally thankful to my tutor Ing. Zbyněk Syrovátka for giving guidance in GT-power with a friendly attitude and for timely remarks which made complex decisions easier. I would like to thank my entire family for their love, support and understanding throughout the duration of my master's studies.

Abstract

The thesis deals with the Design of an additional gas supply into the pre-chamber for a 4-cylinder gas engine. 3-D CAD model and manufacturing drawings of the gas rail were created using the PTC Creo software. GT-power software was used to design the 4-cylinder gas engine model with a scavenged pre-chamber. Simulations were performed to analyse the Model. Based on data from the simulations in GT-Power, the pressure pulsations of the gas rail were studied in the range of engine operation modes. A sensitivity analysis on the size of the gas rail was carried out to propose the best solution to eliminate the pressure pulsations.

Keywords: Pre-chamber, gas rail, pressure pulse, GT-POWER, Scavenging, Natural gas.

Anotace

Diplomová práce se zabývá návrhem dodatečné dodávky plynu do předkomůrky pro 4-válcový plynový motor. Pomocí softwaru PTC Creo.3-D byl vytvořen CAD model a výrobní výkresy plynového zásobníku. GT-Power software byl použit pro návrh modelu plynového 4-válcoveho motoru s vyplachovanou předkomůrkou. Simulace byly provedeny pro detailní analýzu modelu. Tlakové pulzace v plynovém zásobníku byly studovány v rozsahu provozních režimů motoru. Byla provedena citlivostní analýza vlivu velikosti plynového zásobníku pro eliminaci tlakových pulzací.

Klíčová slova: Předkomůrka, plynový zásobník, tlakové pulzace, GT-POWER, Zemní plyn

Contents

Nomenclature

2D	Two dimensional
η	Thermal efficiency
3D	Three dimensional
γ	Specific heat ratio
r_c	Compression ratio
w_t	Turbine specific work
w_c	Compressor specific work
c_p	Specific heat capacity
π	Pi
BSFC	Brake specific fuel consumption
CNG	Compressed Natural gas
CO	Carbon Monoxide
CO_2	Carbon Dioxide
CH_4	Methane
DI	Direct injection
DPC	Developer pre-chamber
ECU	Electronic control unit
EGR	Exhaust Gas Recirculation
GR	Gas rail
GHG	Greenhouse gas
h	Height
HC	Hydrocarbon
LNG	Liquefied Natural Gas
MEP	Mean effective pressure
NG	Natural Gas
NO	Nitric Monoxide
NO_2	Nitrogen Dioxide
NO_x	Oxides of nitrogen
P_{gas}	Actual pressure of the gas

P_0	Standard pressure
PID	Proportional integral derivative
r	Radius
RPM	Revolutions per minute
SI	Spark ignition
T_{gas}	Actual temperature of the gas
T_o	Standard temperature
TDC	Top dead centre
V_{gas}	Cumulative volume into the pre-chamber per cycle
VGT	Variable geometry turbine

Chapter 1 Introduction

1.1 Problems in transportation sector

The transportation system is one of the dominant factors influencing the socio-economic modern society. Though there might be several advantages of using automobiles, depletion of energy sources and pollution remain to be a major consequence of this industry. From the recently published data [1] plotted in Figure 1, CO_2 is a primary GHG (Greenhouse gas) emitted. 76% of the GHG is CO_2. Methane and NO also contributes 16% and 6% of the GHG. These GHG apart from depleting the ozone layer in the stratosphere [26], also pose health hazards to living organisms on this planet [2].

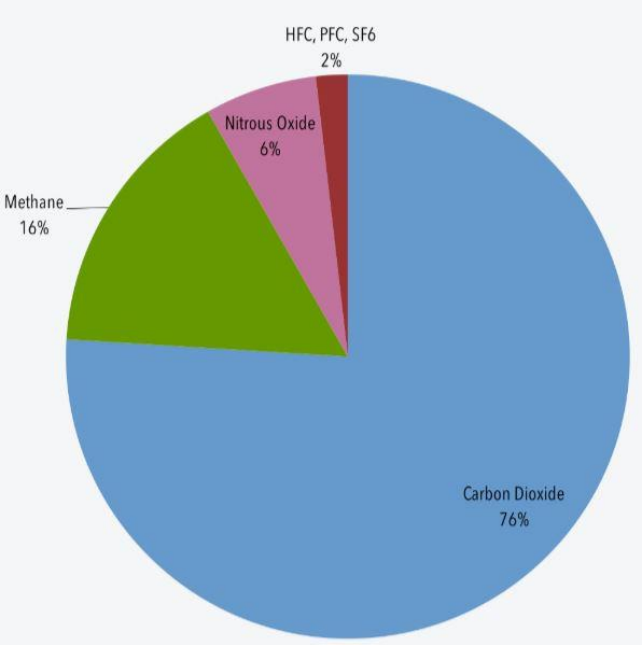

Figure 1 GHG emission composition [1]

The combustion of fossil fuels like diesel and gasoline by the automotive sectors are one of the main sources of CO_2, NO and HC. The Figure 2 shows that contribution of the automotive sector to the total GHG emissions is around 15 %. The main challenge of the automotive manufacturers is to build a more efficient, economic vehicle with relatively less emissions.

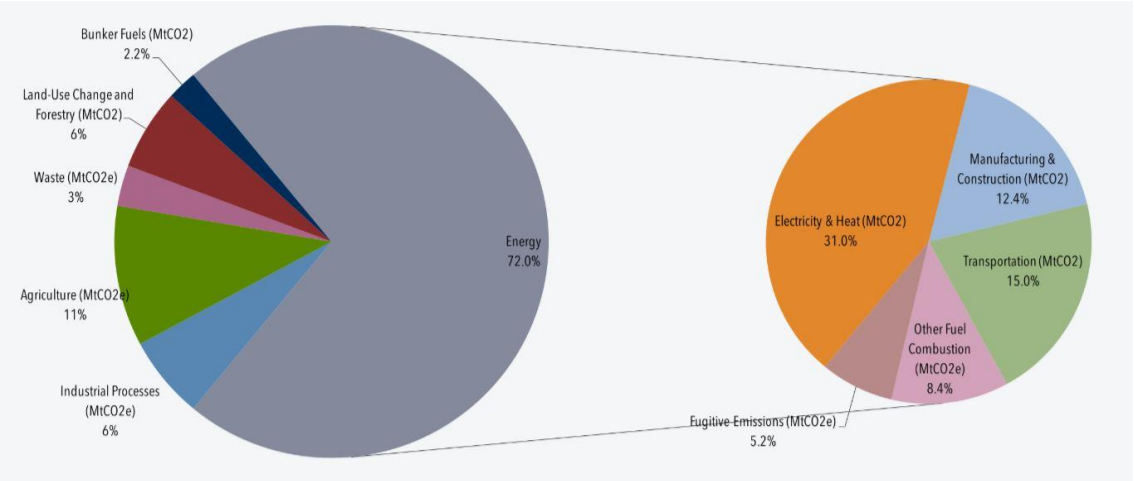

Figure 2 CO2 emission source [1]

1.2 Natural gas as an alternative fuel

NG (Natural gas) is an odourless gaseous mixture of HC mainly made up of CH_4. Two forms of natural gas are used in vehicles: compressed natural gas (CNG) and liquified natural gas (LNG). CNG is produced by compressing natural gas to less than 1% of its volume at standard atmospheric pressure. LNG is natural gas in its liquid form. Purifying natural gas and super-cooling it to -260°F produces LNG [3].

The composition of the NG can vary depending on the deposit and this affects the performance and emission characteristics of the engine [5]. The manufactures must be able to develop an engine which must have fuel flexibility. In [6], the influence of NG composition on engine performance has been assessed at laboratory of the Josef Bozek Research centre for a 4-cylinder turbocharged SI engine. From the research [6], it can be noticed that addition of gas with higher HC slightly increases the engine power and efficiency but worsens the knock resistance of the fuel and slightly increases the CO_2 emissions. The addition of hydrogen worsens the knock resistance of the fuel, decreases the engine power and efficiency, but effectively decreases the emissions of CO_2. NG has higher octane number, which means it is more resistant to knock. Since it is more resistant to knock, it can be used in engines with higher compression ratios than conventional SI engines. Thus, NG can achieve a greater thermal efficiency than the conventional fuels when used in a SI engine [17].

When energy consumption and GHG emissions of gasoline, diesel and NG were assessed, it was observed that NG are more efficient than the former two fuels [4]. NG in vehicles has proved to achieve low emissions which shows that it has the potential to be very environment friendly. With energy consumption of the transport industry increasing by each passing year and consequently the fuel prices of gasoline and diesel being higher than NG along with growing awareness in cutting GHG, NG could be a well prospective fuel in the future [27] [28]

1.3 Research motivation and scope

When an NG engine runs in extremely lean homogenous mixture, it leads to low combustion temperature and much further reduction in NO_x emissions (lean burn concept) [8]. Also, additional air in the lean mixture increases the specific heat ratio which leads to increase in thermal efficiency [9]. When operating in extremely lean mixture, it leads to lower burning speed, high HC emissions and poor combustion stability. Many researchers have been working to come up with new strategies to increase burning speed of an NG SI engine. One such strategy is to use a different kind of ignition system. One of such ignition concepts is the implementation of pre-chamber ignition.

Therefore, the motivation for the research presented is connected to work of my predecessors [8], [10] which emphasises the application of scavenged pre-chamber ignition system in light duty truck gas engine as an alternative to the conventional SI method.

Goals of this thesis are as follows:

- To give an overview on the essential background concepts and highlight the important studies that support the pre-chamber ignition system in NG engines.
- To elaborate about the experimental engine and setup.
- To create a design of a GR (Gas rail) to supply additional gas to the pre-chamber and produce 3-D models and drawings of it.
- To create a GT-POWER model of a 4-cylinder scavenged pre-chamber gas engine. Modify the model so that it is like the experimental setup. Calibrate the GT-

POWER model with data from the experimental engine. Calculate the engine performance map of the model.

- To analyse the effects of scavenging in the pre-chamber. To study the pressure pulsations in the working range of the GR and perform sensitivity analysis on the dimensions of GR.

Chapter 2 Literature review

2.1 Emissions in SI engine (air/fuel equivalence)

Air excess is an important factor in SI engine emissions. The factors that affect emissions which are controlled by the air excess ratio, are the oxygen concentration and the temperature. Figure 3 shows the effect of lambda on SI engine. It indicates that, if the engine can be operated in sufficiently lean condition, the engine could get low fuel consumptions and control engine emissions. However, such a lean combustion approach requires a fast burning combustion [9]. The Figure 3 shows the variation of brake specific fuel consumption, NO, and HC with air/fuel and fuel/air equivalence ratio [16].

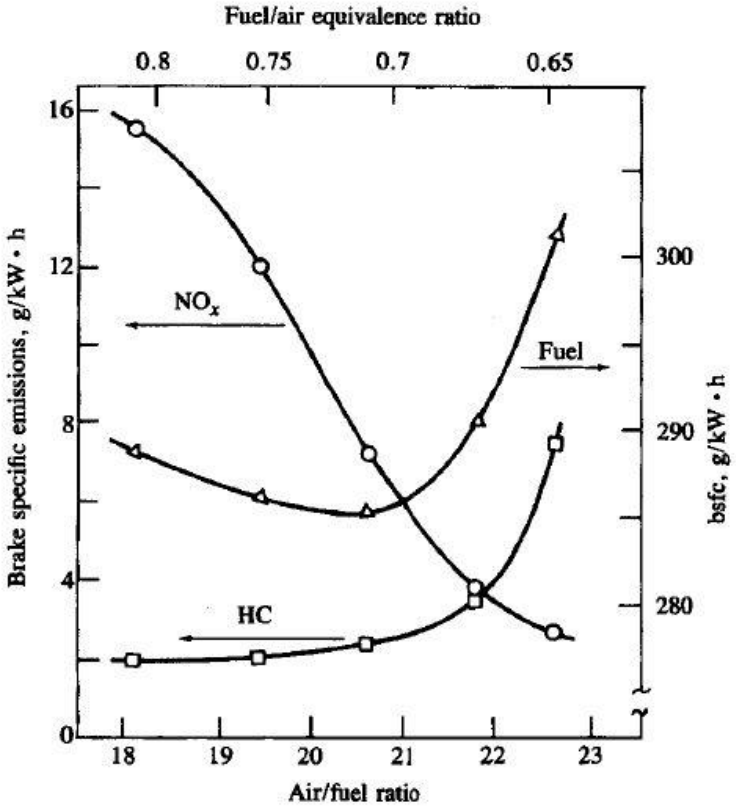

Figure 3 Variation of brake specific fuel consumption, NO and HC emissions with air/fuel and fuel/air equivalence ratio [16]

2.2 Lean burn concept

It can be clearly seen from the above section that if the engine is operated in lean condition, then there is a reduction in NO_x emissions. However, the NO rises initially and then reduce drastically. Lean burn occurs when the air/fuel (A/F) ratio or lambda is greater than 1 i.e., additional air is added to the mixture, when compared to the stoichiometric A/F ratio. And this increases the specific heat ratio of the mixture which leads to increase in thermal efficiency from the equation (1) [10] [9].

$$\eta = 1 - \frac{1}{r_c^{(\gamma-1)}} \quad (1)$$

Where,

η (%) = Thermal efficiency

r_c = Compression ratio

γ = Specific heat ratio

The lean burn reduces the peak cylinder temperature which reduces heat losses [8]. NO_x is produced mainly due to high temperatures in the cylinders. Therefore, low temperatures of the combustion due to lean mixture produces lower level of NO_x emissions. Lean burn concept reduces the fuel consumption of the engine. So, it allows the engine to run less throttled with same power output by reducing the throttling and pumping losses. Apart from the decrease in fuel consumption, it also decreases the probability of knocking which results in possibility to operate at a high compression ratio, which delivers higher thermal efficiency. Lean burn concept can be implemented in conventional SI engines as it has low engine efficiency in part load operation condition [17].

Despite the advantages of the learn burn concept, there are several problems in the use of lean burn concept. The drawbacks are low burning rate and lower flame speed, which results in increased combustion duration. The slow burning doesn't allow complete combustion before the opening of the exhaust valves. Due to this fact the misfire limit is reached. Due to the misfire in the engine, there is an increase in the level of cycle to cycle combustion variation. This obviously decreases the efficiency, increases torque variations and HC emissions in the engine [9].

The drawbacks of low burning rate can be overcome by making the burning fast and stable. This can be achieved by using any of the following methods - creating high

turbulence, high compression, turbocharging and using advanced combustion techniques [11].

2.3 Stratified charged concept

There are 2 conditions involved with respect to charge mixture during combustion process – homogeneous and stratified charge mixture. These types of mixtures are dependent on the time of fuel injection. Homogeneity is acquired when the charge is injected earlier so that there is enough time for proper mixing of fuel. The amount of air going inside is controlled by using throttle or variable intake valve according to the fuel injected, to maintain the right air to fuel ratio. The constriction of air flow causes pumping losses in the system and to overcome this loss, the air is taken in through the port and the fuel is injected in the combustion chamber late in the compression stroke to have a readily ignitable mixture near the spark plug for ignition. As giving more time can make the charge get excessively diluted. This is known as the stratified charge engine. Due to DI during later stages of compression strokes, the knock problem is avoided. This makes this concept more fuel tolerant and possible to work with a wide range of fuels.

There are many types of stratified charged engines. Few stratified charged engines have the piston top in the shape of a bowl. This bowl-in-piston increases the degree of air swirl created during intake stroke and compression stroke and enhances the mixing of air and fuel. The fuel is injected tangentially into the bowl during the later stage of compression stroke. This propagates the downstream flame and quick burning of the fuel air mixture. Figure 4 shows the examples of two stratified charged engines used in commercial practice: Texaco controlled combustion system and the M.A.N FM system [9] [11] [18]

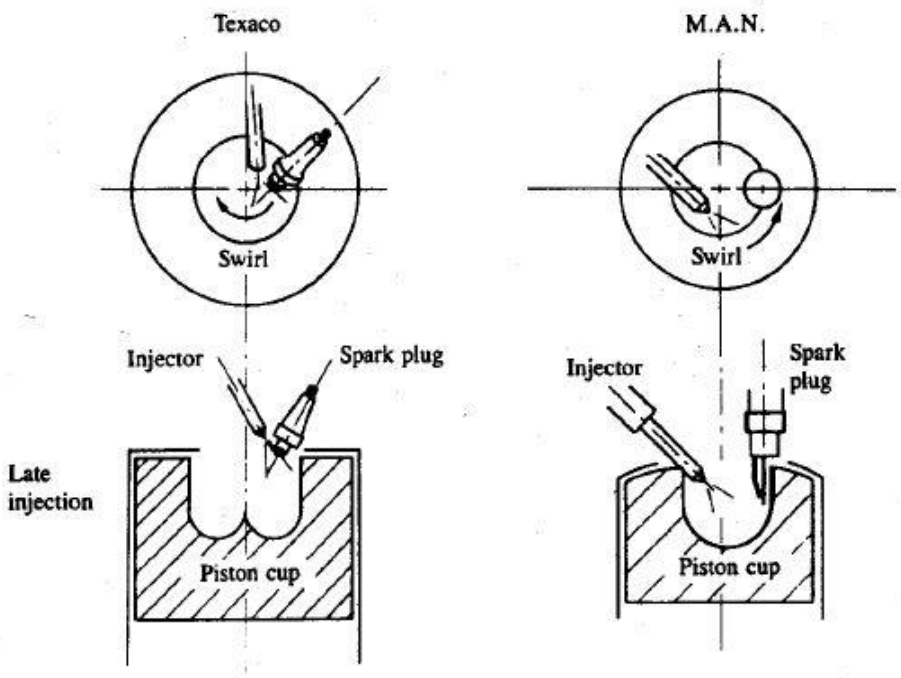

Figure 4 Two stratified charged engines used in commercial practice: Texaco controlled combustion system and the M.A.N FM system [9]

2.4 Pre-chamber concept

An alternative stratified charge concept is the Pre-chamber concept. This concept of the pre-chamber was first presented and patented by Sir Harry Ricardo in 1918. In this type of system, there is a small chamber (pre-chamber) connected to the main chamber. The pre-chamber has its own supply of fuel air mixture. The spark plug is placed in the pre-chamber. During the intake stroke the pre-chamber is filled with rich mixture and main chamber is filled with lean mixture. When the compression starts, the lean mixture moves into the pre-chamber and forms an ignitable, slightly rich mixture near the spark plug. When the ignition starts in the pre-chamber, the flame developed comes as a jet into the main-chamber igniting the lean mixture in the chamber thus being called jet ignition. This increases the lean mixture operation range of the engine. Its operation is shown in Figure 5 [9]

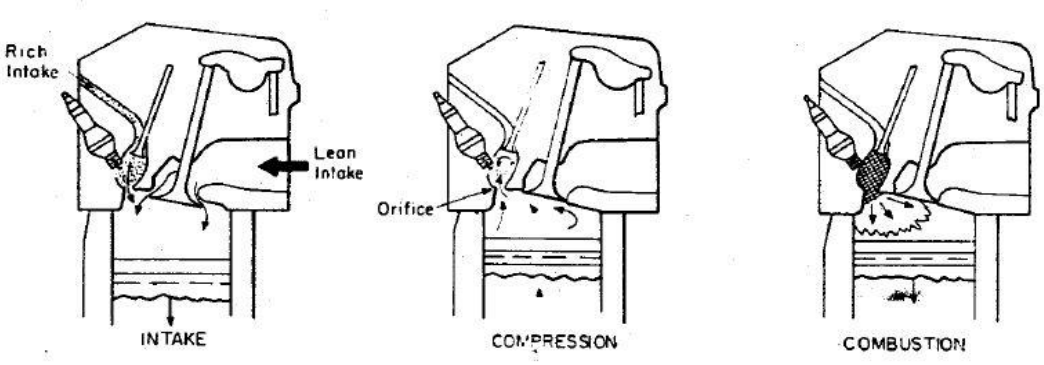

Figure 5 Operation of pre-chamber engine [9]

One of latest development of the pre-chamber ignition system was patented by Mahle Powertrain in 2014 and named it as Turbulent Jet Ignition (TJI). Figure 6 shows the cross-section of Mahle powertrain TJI system [24]. This system has a small pre-chamber and two separate injectors to fuel the main and pre-chamber. The spark plug, along with one of the injectors are placed in the pre-chamber housing. The rich fuel supplied to the pre-chamber is ignited by spark plug and the partially combusted fuel is forced through the orifices of the pre-chamber into the main chamber, burning the main chamber fuel mixture. When the engines are operated with TJI, they have more thermal efficiency and can be operated up to air access of 2.1, which is more compared to standard ignition system with only 1.4 as seen from the Figure 7. The combustion stability of the TJI is better than the conventional ignition system observed from Figure 8. The NOx emissions are considerably lower in TJI with levels lower than 10 ppm when operated in air excess of more than 1.8 from Figure 9.

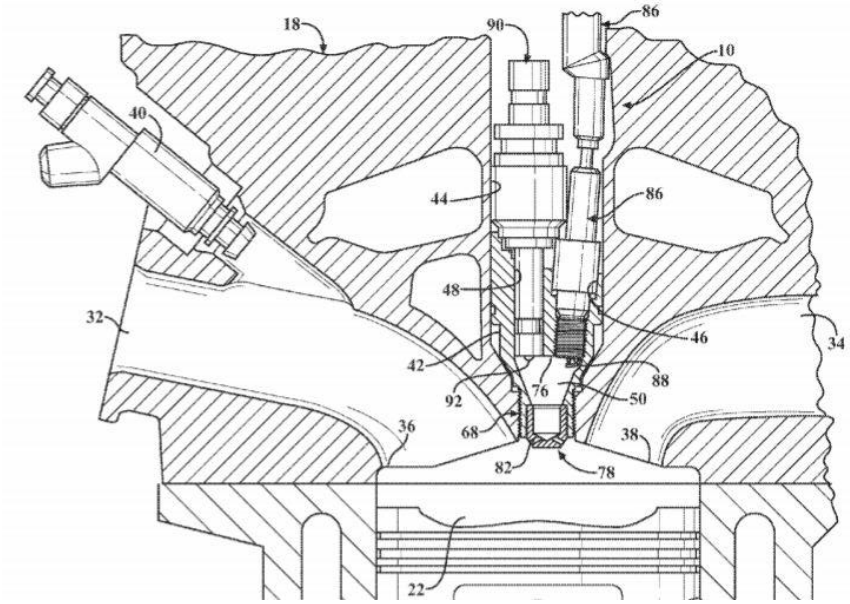

Figure 6 The cross-section of Mahle powertrain TJI system [24]

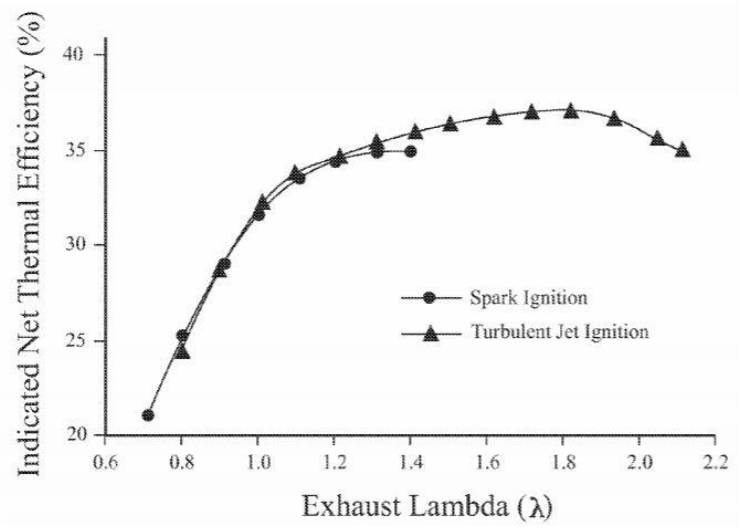

Figure 7 Indicated thermal efficiency vs exhaust lambda [24]

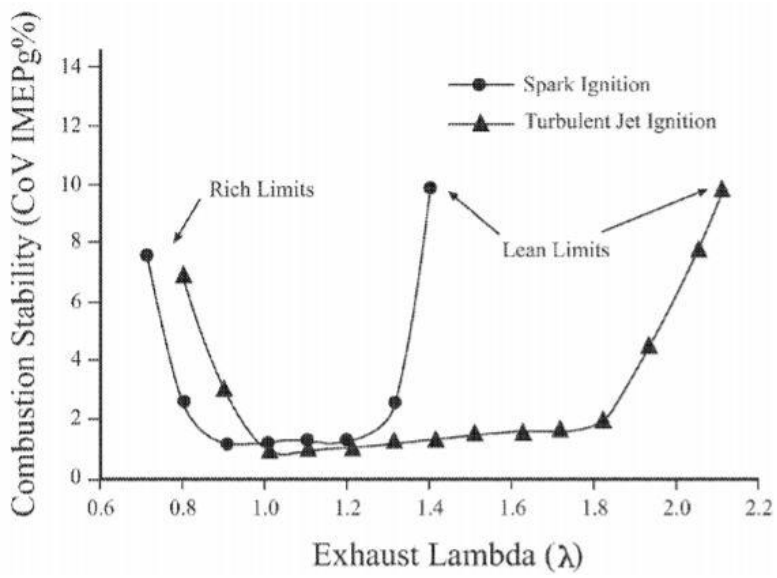

Figure 8 Combustion stability vs exhaust lambda

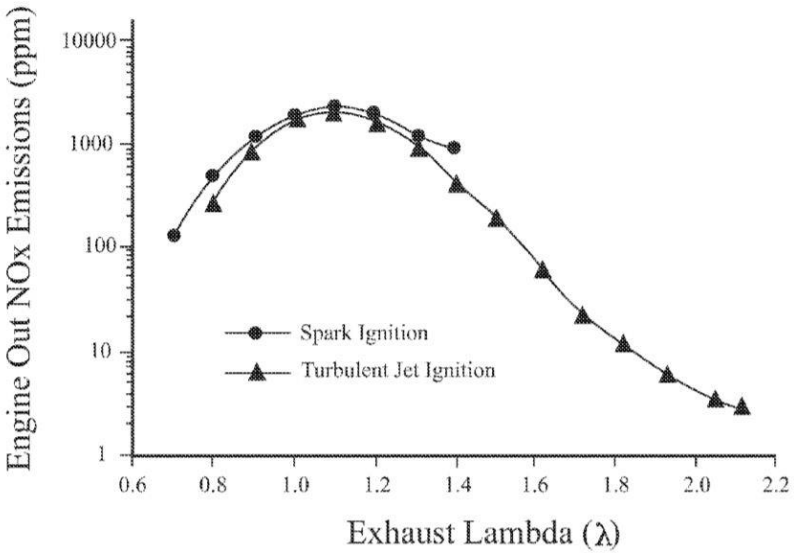

Figure 9 NO_x emissions vs exhaust lambda

The TJI system can be fuelled in the main chamber and pre-chamber with various fuel combinations between them like - gasoline-gasoline, gasoline-propane, Gasoline-Vaporized gasoline, gasoline-natural gas and natural gas-natural gas [29]. *NG* is seen as a potential alternative which is cheaper than conventional fuels, with higher knock resistance and lower CO_2 emissions. When natural gas is used in both pre-chamber and main chamber in the TJI system, it gives lean operation range same as that of gasoline fuelled TJI [30]. But, the fuel economy is at its optimum when operated with natural gas-natural gas when compared to other combinations which can be seen in Figure 10 [29].

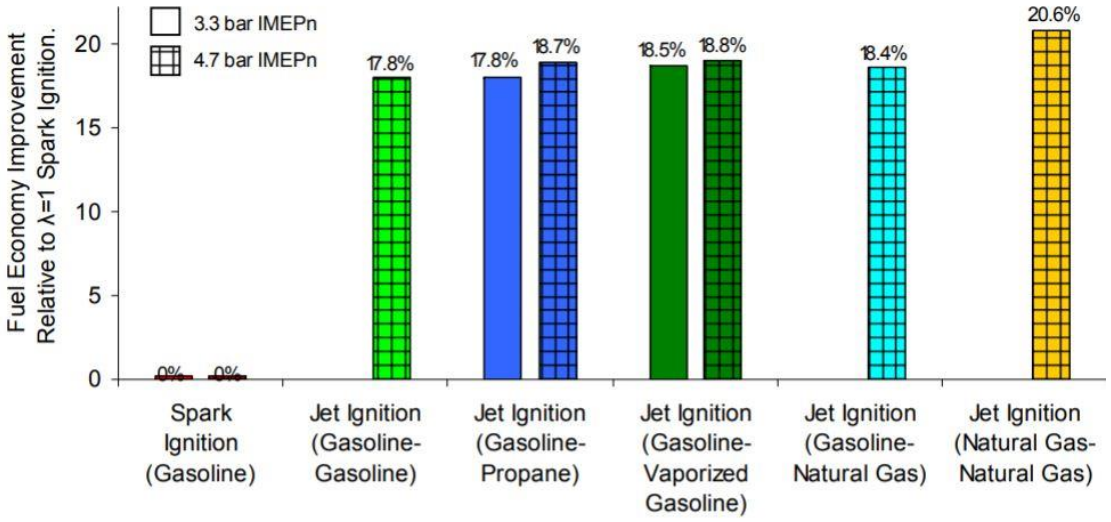

Figure 10 Relative fuel economy improvement relative to SI ignition vs different fuel combinations for TJI system [29]

MULTITORCH GmbH introduced spark plug with pre-chamber housing in 2012. This system has the pre-chamber and spark plug as one component. This can be replaced with the conventional spark plug. The cylinder head need not be modified as the threading of the pre-chamber spark plug and the conventional are kept same These have longer service life when compared to conventional spark plug types. The ignition electrode comprises multiple electrode arms which creates an electric arc. The spark plug housing for the pre-chamber has no separate fuel supply, so it is not scavenged. While the compression stroke, the fuel goes inside the pre-chamber from the main chamber. After the spark, there is an increased flame growth which comes as jet into the main chamber, burning the main chamber fuel. The disadvantage of this type is that the burned gases in the pre-chamber are not scavenged so some residual gas remains in the chamber. Figure 11 shows the cross-section of MULTITORCH GmbH pre-chamber spark plug with housing [23].

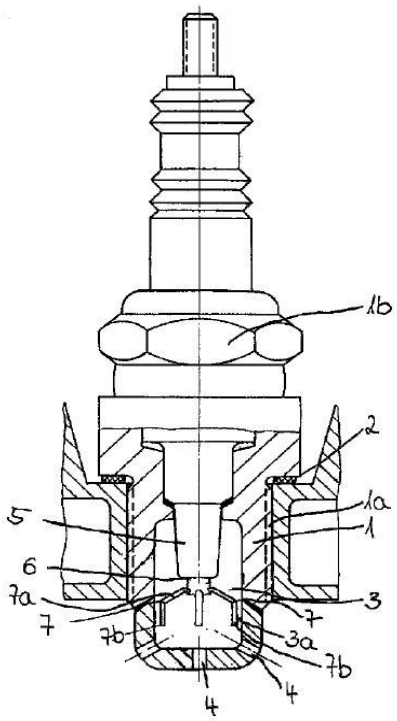

Figure 11 The cross-section of MULTITORCH GmbH pre-chamber spark plug with housing [23]

Seeing the future demand for NG engines, Pre-chamber spark plug for NG engine was developed by DENSO Corporation. When the DPC (developed pre-chamber) plug was experimented in the study [31], it was observed that the combustion stability was better for DPC plug and it can be operated up to air access of 1.95, which is more compared to standard ignition system with only 1.85 seen in Figure 12. From the Figure 12, there is an improvement thermal efficiency and the NOx emission level when compared to the standard plug.

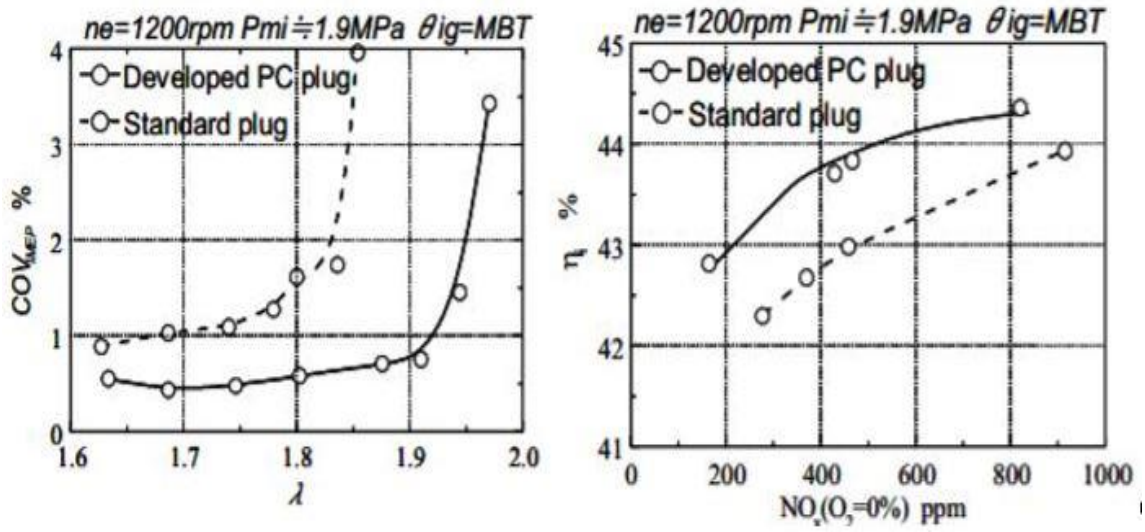

Figure 12 Combustion stability vs lambda (left) and thermal efficiency vs NO_x emission level (right)

Chapter 3 Experimental setup

3.1 Experimental engine

The experimental setup was in Czech Technical University Lab in Josef Bozek Research Centre for Vehicles of Sustainable Mobility. The experimental setup has already been developed by predecessors [6][8]. All the modifications for the engine were made in-house.

The engine in the setup is a 4-cylinder 4 stroke light duty truck NG engine. The engine has a bore and stroke of 102mm and 120 mm, respectively. The displacement volume of the cylinder is 3.92 dm^3 with a compression volume of 80cm^3. The engine is turbocharged with an intercooler and a compression ratio of 12. The Turbo charger model is CZ-C14 which has VGT controllable by the ECU. There is a central mixing unit for feeding the gaseous fuel into the compressor. It is possible to control the lambda using the conventional oxygen sensor which is integrated with the ECU. The throttling is controlled by the throttle valve actuated by the stepper motor which is controlled by the ECU. A capacitive ignition system (UNIMA TC+) allows independent varying of the spark timing. All the actuators and the sensors are coupled to the ECU developed by predecessor [6] using a field programmable gate array as a platform. The engine is coupled to a DC dynamometer with which the engine can be loaded. The main parameters of the original SI engine arrangement are given in the Table 1[6] [12]

No of cylinders	4
Bore	102 mm
Stroke	120 mm
Displacement	3.92 dm^3
Compression ratio	12:1
Maximum Power	125 KW @ 2400 - 2800 RPM
Maximum Torque	600 Nm @ 1500 – 1600 RPM
Charging	VGT turbo charger with intercooler

Table 1 Main parameters of the original SI engine arrangement [6]

The experiments were performed by converting the Original engine into a single cylinder engine by closing the intake and exhaust runners with metal plates. Figure 13 shows the scheme of the test engine layout with redlines indicating the intake and exhaust runners closed with plates.

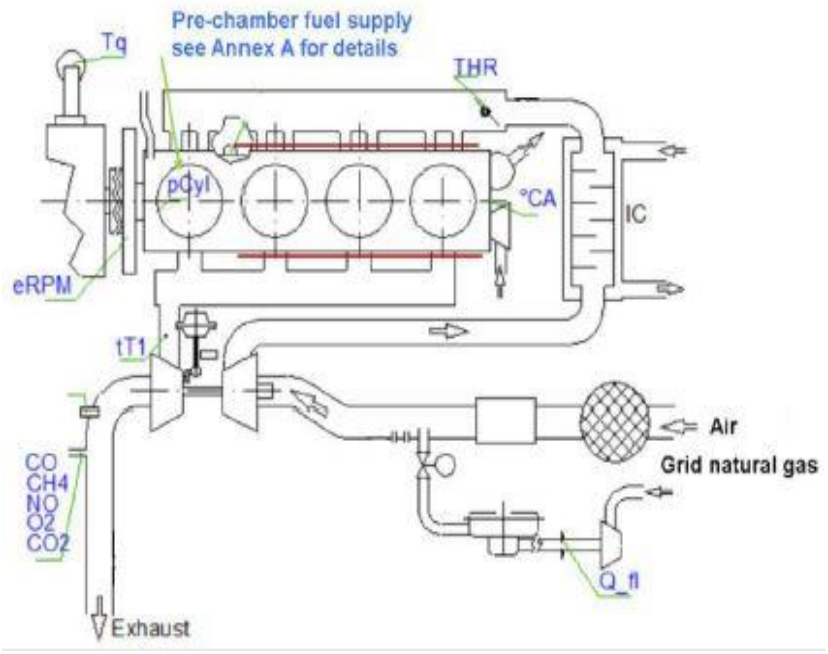

Figure 13 The scheme of the test engine layout [8]

3.2 Pre-chamber design

The module of pre-chamber assembly was designed and manufactured by predecessor [8] in a such a way that the size, geometry and number of orifices of pre-chamber can be modified and experimented. The pre-chamber module is cylindrical in shape. The pre-chamber housing protects the gas pipeline inside, the sparkplug and ball check valve. Standard sparkplug (Brisk CR10YS) is used. The pre-chamber is installed with an uncooled AVL GH15D pressure transducer. The cylinder head of the engine was modified in such a that the pre-chamber module can be fitted and taken out. The pre-chamber module cross-section and cross-section of the cylinder head with pre-chamber module as shown in Figure 14.

Different pre-chamber geometry and jet nozzles were tested in the engine under steady state operation by the predecessor [8]. The pre-chamber with the largest volume and greatest cross-section area of the nozzle showed the best efficiency and low *HC* and NO_x

emissions. For experimental work in this thesis the pre-chamber was replaced by a pre-chamber with a bigger volume. The parameters of the pre-chamber and nozzle design is given in the Table 2 and with more details in Attachment A.

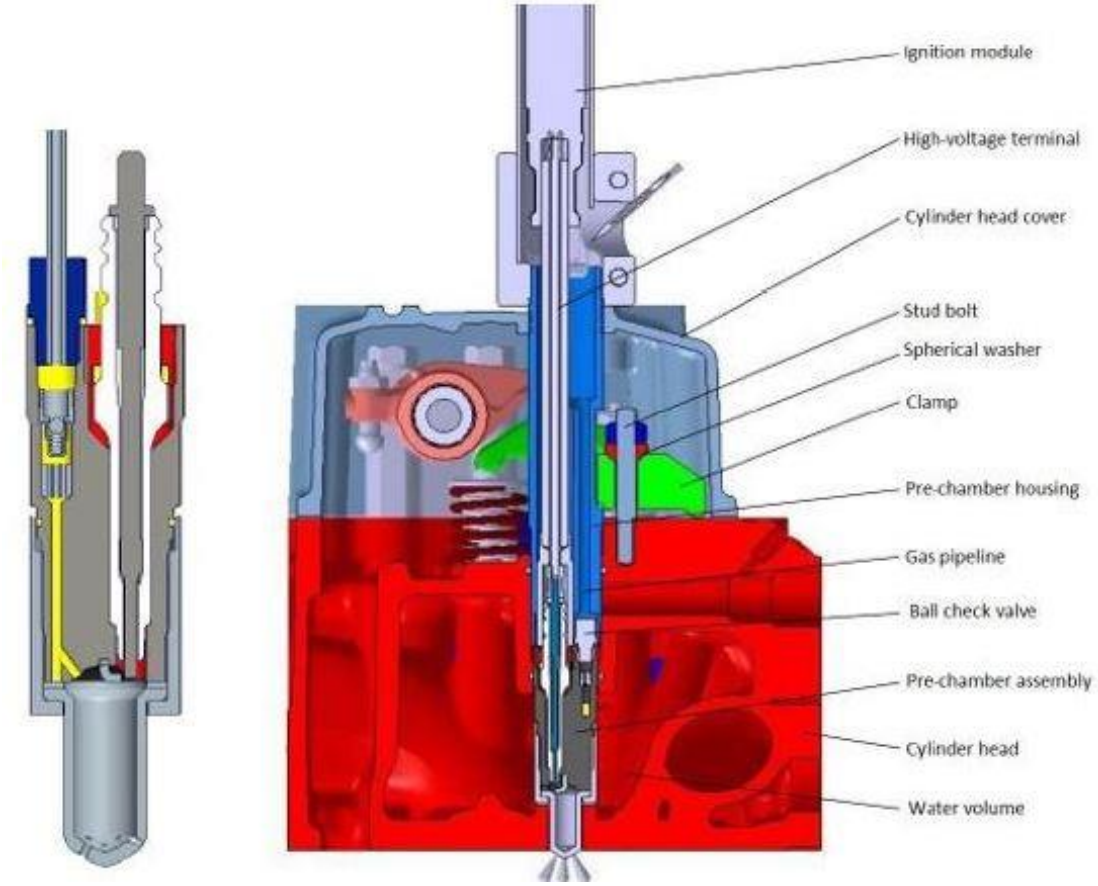

Figure 14 The pre-chamber module cross-section (left) and cross-section of the cylinder head with pre-chamber module (right) [21]

Volume	4.1 cm^3
Fraction of compression volume	5.12%
Number of holes	12
Hole diameter	1.2mm

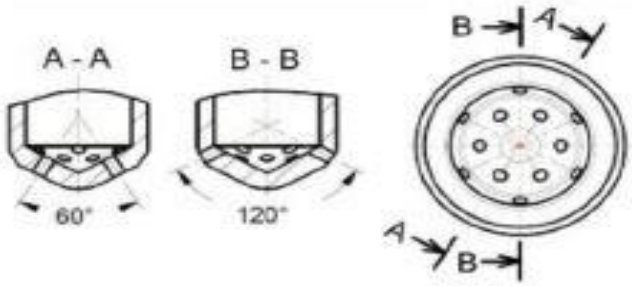

Table 2 The parameters of the big pre-chamber and nozzle design

3.3 Gas supply line to the Pre-chamber

The additional fuel is supplied by *CNG* gas line in the laboratory with pressure going up to 200 bar in the line. The pressure from the gas line is reduced by a pressure regulator. Fuel flow to the pre-chamber is controlled and measured by a mass flow meter OMEGA FMA2610. The fuel then passes through a rotameter with which the average volumetric flow can be inspected. The fuel then goes through a damping vessel and then finally into the pre-chamber through a check valve. The schematics of the additional gas supply line to the pre-chamber can be seen in Attachment B.

Chapter 4-Design Part

The damping vessel in the schematics of the additional gas supply line to the pre-chamber which can be seen in Attachment B was replaced by a GR. There are some basic requirements the GR design must fulfil. The engine dimensions and the placement of the gas supply line into the GR are the main consideration taken to fix the basic dimensions. The GR must have a safety feature to work in case of very high pressure in the system. A device must be placed to measure the pressure inside the system. It must be designed using components from the instrumentations fittings manufacturers which are easily available. The chapter is divided into 2 main parts, the first part gives the basic idea for the design and the second shows how the design was implemented by using mass manufactured instrumentation fittings and sensors with 3D Model and drawings. The models and drawings of the GR were created using the PTC Creo software.

4.1 Gas rail design

The GR must be fitted with a pressure sensor to sense the pressure in the rail and with relief valve which releases the pressure from the system in case the threshold safety pressure level is reached. The GR consists of 3 main parts, which include plenum, runners and intake runner. The gas enters the plenum through the intake runner, plenum stores the fuel and then sends it to the pre-chamber through the runners. plenum is a storage device which is placed between the intake runner and the runners. The plenum volume is larger than the intake runner and the runners. The function of the plenum is to store the fuel and equalize the pressure because of irregular demand by the pre-chamber. The plenum helps in even distribution of the fuel to the chamber. The plenum is highlighted in red in Figure 15 of the basic layout of GR.

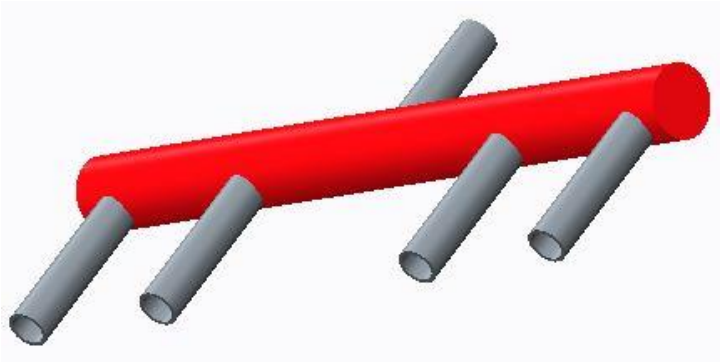

Figure 15 Basic layout of the GR (plenum highlighted in red)

Intake runner is the part that delivers the gas in to the system. The gas from the laboratory supply line comes to the plenum area through the intake runner. The intake runner is highlighted in red in Figure 16 of the basic layout of GR. The runners are that part of the GR which delivers the gas to the pre-chamber from the plenum area. The runner governs the equal distribution of fuel by eliminating the pressure pulsation created due to irregular demand by pre-chamber from reaching the plenum area. The runner is highlighted in red in Figure 17 of the base layout of the GR.

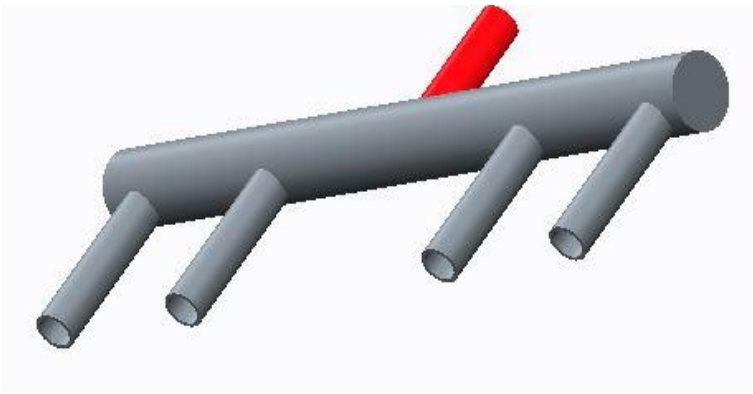

Figure 16 Basic layout of the GR (intake runner highlighted in red)

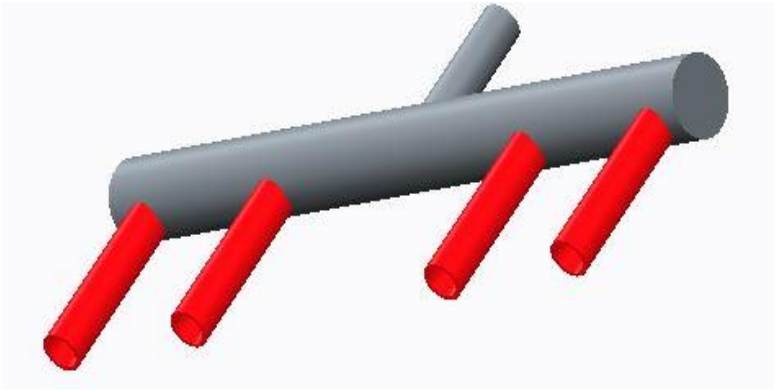

Figure 17 Basic layout of the GR (runners highlighted in red)

4.2 Implementation of the base Gas rail design

The idea of the design is implemented using mass manufactured instrumentation fittings which are easily available, robust and cheap. The GR and the experimental engine is in the developing stage, so it is better to use instrumentation fittings because it can be removed, and different sizes can be implemented easily. If each time the GR with different dimension must be manufactured, it will be expensive and consume more time. The experimental setup dimensions were measured, and the fittings were selected from instrumentations fitting company to assemble the GR. The fittings selected were ensured that it had enough pressure withstanding capacity and have threading which are compatible with each other. The pressure sensor and pressure relief valve chosen are robust and under the working range of the GR. The chosen components for the assembled GR is given below in the Table 3.

Component make	**Component name**	**Model name**	**Quantity**	**material**	**Pressure rating**
Superlok	female tee NPT thread	IFT-8N	5	SS316	351bar
Superlok	Hex nipple male NPT Threads	IHN-8N	4	SS316	530bar
Superlok	Male adapter	SMA 8-8N	5	SS316	-
BD sensors	-	DMP 331	1	-	60 bar
Superlok	-	SRVL-MS-8N-8-Y-SS.	1	-	20.6 bar

Table 3 Bill of materials to assemble the GR unit

All parts mentioned above are assembled together. The five male adapters are fixed with perpendicular opening of all the female tees. The female tees are connected in-line with the help of four male hex nipple. The pressure sensor is fixed with assembly in one end and the relief valve is fixed with the assembly in the other end. Female tee with the male hex nipple which supply fuel to the pre-chamber must be aligned and inline. The length of the GR without the pressure sensor and relief valve is approximately 530 mm which is suitable to the engine dimensions.

The plenum has a volume of 119.16 cm^3. The runners have a length and diameter of 50.8mm and 9.4 mm. The total volume of the GR is calculated to be around 136 cm^3.The

Figure 18 shows the picture of a 3-D drawing of assembled GR and the manufacturing drawing is attached in Attachment C. The red arrow in the Figure 18 indicates the flow of gas in to the GR from the laboratory gas supply. The blue arrows indicate the flow of gas to the pre-chambers.

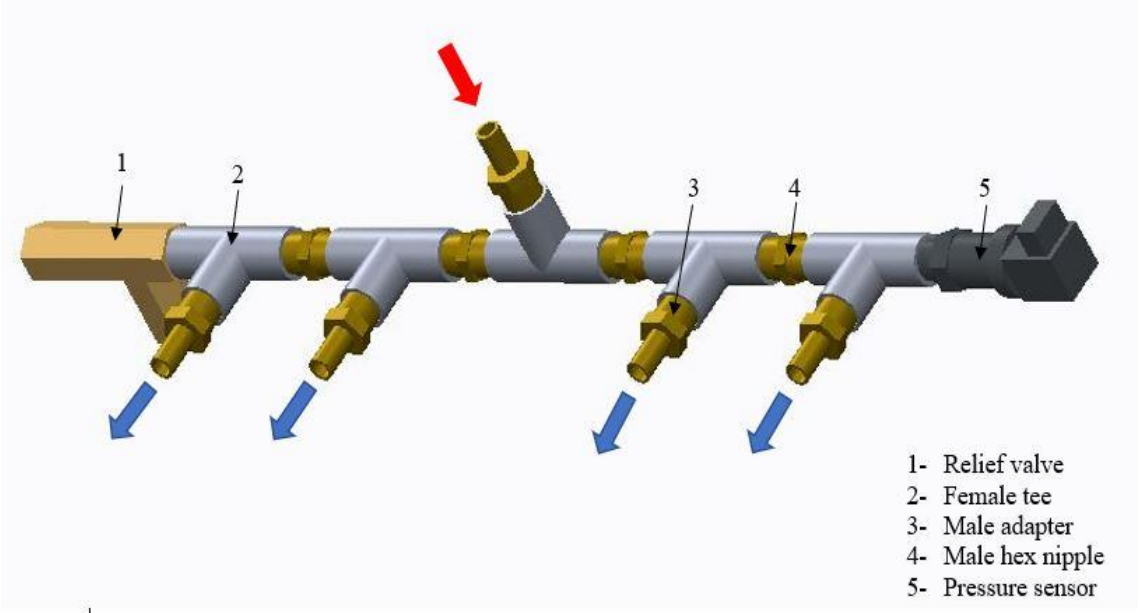

Figure 18 3-D drawing of assembled GR indicating the flow of gas into the GR from the laboratory gas supply (red arrow) and the flow of gas to the pre-chambers (blue arrows)

Chapter 5 GT-POWER Part

A GT-POWER model of the single cylinder gas engine with scavenged pre-chamber by the predecessors can be seen in the Attachment D. The pre-chamber is Considered as a separate cylinder attached to the main chamber through the orifice by the GT-POWER. The combustion model was given for the main-chamber and the pre-chamber separately in the model. The settings, boundary conditions and dimensions of the model is set same as that of the experimental engine by the predecessor [12]. This chapter has the following parts:

- Modelling of a 4-cylinder model with scavenged pre-chamber from the single cylinder model. The GR was added to the model with the designed dimension, layout and proper boundary conditions.
- Exploring and understanding the model and making Certain modifications to control the operating conditions of the model while simulating. For example, Exhaust lambda controller was added to control the exhaust lambda in the model during simulation.
- The model was calibrated with data from the experimental engine and then compared to it.
- The Full load characteristics of the created model was compared with data from the 4-cylinder original SI engine. Finally, the performance map of the 4-cylinder model was plotted.

The final 4-cylinder model with the modifications described in this chapter can be seen in the Attachment E for future reference.

5.1 4-cylinder model

The given single cylinder model was converted into a 4-cylinder model. 3 new cylinders and pre-chambers where added to the model with initial state object, heat transfer object,

flow object, combustion model and other characteristics which were same as that of the base model. The volume of the added pre-chambers was 4.1 cm^3.The dimensions of the pre-chamber can be found below in the Attachment A. The designed GR was added to the model with the dimensions that are mentioned in chapter 3. The supply to the GR is from the end environment which represents the supply line from the laboratory. The parameters that can be changed in the 4-cylinder model by the user for testing different operating setup can be seen in Table 4.

Parameter	Unit	Description
Pressure initial	bar	The initial pressure (absolute) for the experiment setup
Temperature initial	K	The initial temperature for the experiment setup
Gas supply pressure	bar	The GR pressure from the end environment which is the laboratory gas supply line
Intake Lambda		Air excess in the intake manifold
CA50 pre-chamber	degree	The specified angle is the degree between TDC and typically the 50% combustion point of the Wiebe curve (for pre-chamber).
CA50 Main	degree	The specified angle is the degree between TDC and typically the 50% combustion point of the Wiebe curve (for Main chamber).
CA10-90 pre-chamber	degree	Duration of the Wiebe combustion curve of the pre-chamber
CA10-90 Main chamber	degree	Duration of the Wiebe combustion curve of the main chamber
Engine speed	RPM	Engine speed
Throttle angle	degree	Throttle angle (0-closed to 90-fully open)
Turbine rack position		Turbine Rack position (0-full boost and 1-no boost)

Table 4 The parameters that can be changed in the 4-cylinder model by the user

5.2 Modification of the 4-cylinder model

There are some criteria the model must fulfil to work like the experimental engine. This section's aim is to make some modification in the model to fulfil the criteria. The criteria are as follows:

- There must be a provision to control the average gas flow rate into the pre-chamber by the user in the case setup.
- The lambda in the Exhaust chamber must be controllable by the user in case setup.
- There must be a provision to control the IMEP output of the model and switch off or on this controller according to user's wish.

- There must be a provision to control the EGR percentage going into the intake in the model.

The first simulation was performed to study the sensitivity of the gas flow into the pre-chamber, depending on the gas pressure for different engine speed. The model was simulated at three engine speeds -1200, 1800, and 2400rpm at gas supply pressure of 1.5, 1.7, 1.9 and 2.1 bar. The initial temperature and pressure was set as 298.15 K and 1 bar for all simulations in this thesis. The Model simulation case setup for additional gas supply sensitivity is mentioned below in Table 5.

Parameter	**Unit**	**value**
Intake lambda		1
CA-50 Pre-chamber	degree	-10
CA-50 Main	degree	10
CA10-90 pre-chamber	degree	15
CA10-90 Main chamber	degree	30
Gas supply pressure	Bar	1.5, 1.7, 1.9, 2.1
Engine speed	RPM	1200, 1800, 2400
Throttle angle	degree	90 (full open)
Turbine rack position		1 (no boost)

Table 5 Model simulation case setup for additional gas supply sensitivity

From the results of the above simulation, it was noticed that the gas flow into the pre-chamber is due to the pressure difference between the pre-chamber and GR pressure which is given by the laboratory gas supply line. If the pressure in the pre-chamber is more than the gas pressure, the reverse flow from the pre-chamber into the GR is restricted by the one-way check valve installed. Figure 19 presents the plot of the gas flow rate and GR pressure against crank angle. It is noticed that When the pre-chamber pressure goes below the GR pressure, the gas flow starts. It is evident that in the exhaust stroke, when the pressure in pre-chamber goes up a bit there is a sink in the gas flow rate. A graph is plotted with the gas flow rate to the pre-chamber against the crank angle in Figure 20. Keeping the engine speed constant, if the GR pressure is raised, it can be noticed that the gas flow rate increases. If the pressure is high in the GR, then eventually the difference is also high which creates a greater gas flow rate. The cumulative volume of gas per cycle into the pre-chamber decreases as the RPM increases when the GR pressure is constant. This phenomenon is because when the engine speed is low, there is more time for the gas to flow inside the pre-chamber. Therefore, there is an increase in the cumulative gas volume per cycle into the pre-chamber as the engine speed decreases.

Figure 21 is plot between GR pressure and gas flow rate for various engine. When the engine speed is constant, it is noted that as the GR pressure increases, the gas flow rate increases. When the GR pressure is constant, it is evident in the graph that the gas flow rate decreases as the RPM increases. From the results, gas flow rate to pre-chamber is not constant at all engine speed. Like the experimental setup, the gas supply pressure must be continuously varied to maintain the gas flow rate into the pre-chamber by a controller.

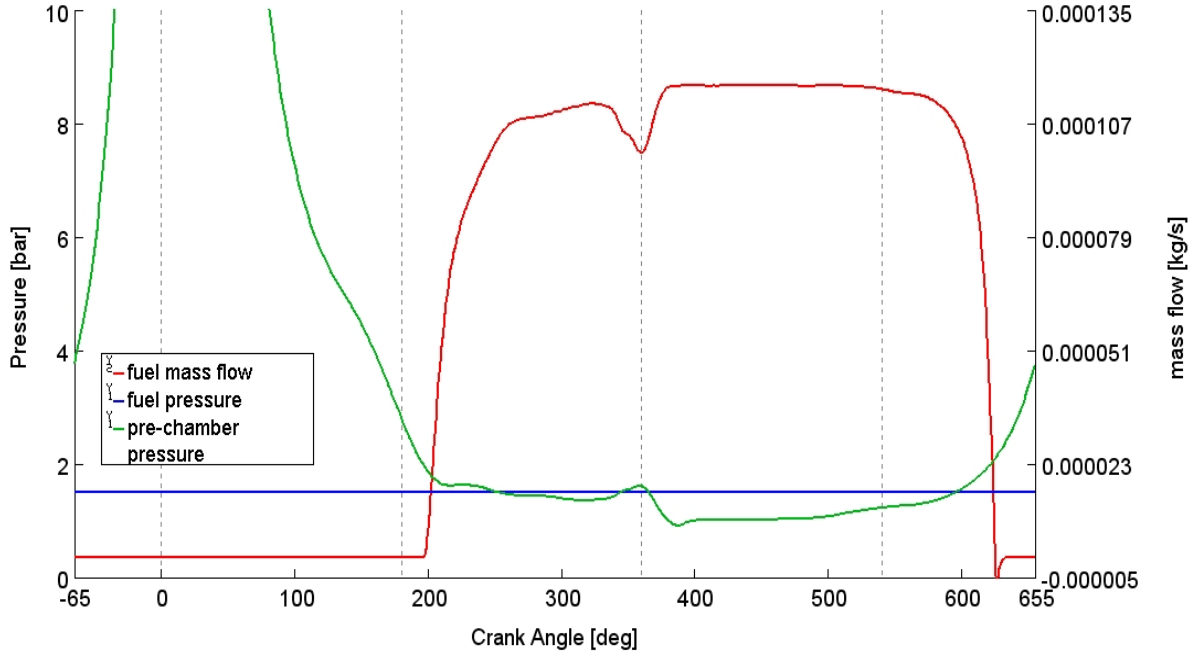

Figure 19 Plot of the gas flow rate into the pre-chamber and GR pressure against crank angle at 1800 RPM

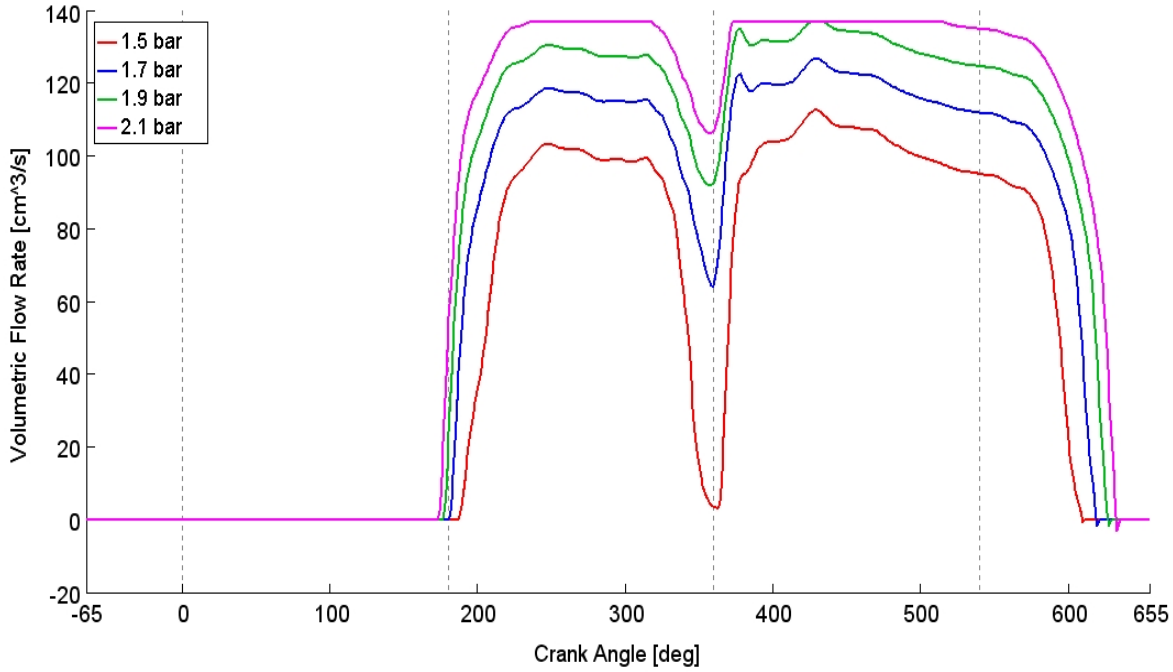

Figure 20 Gas flow rate into the pre-chamber against the crank angle at constant engine speed of 1800 RPM

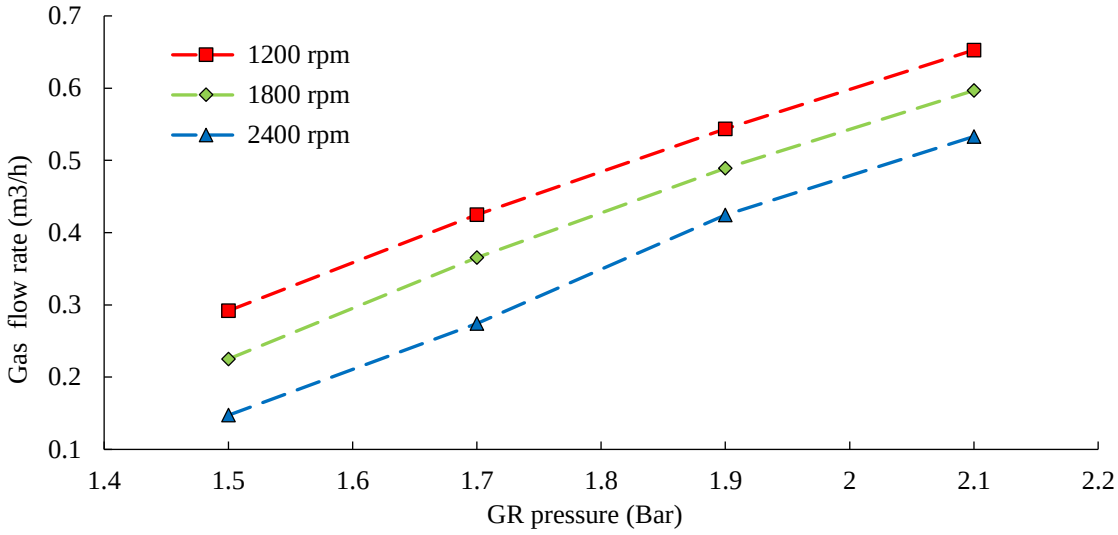

Figure 21 Plot between GR pressure and gas flow rate for various engine speed

5.2.1 Gas Flow Rate Controller

The formula for gas flow rate (m^3/h) 'Q' into the pre-chamber is given below in the equation (2).

$$Q = \frac{3.P_{GAS}.V_{GAS}.T_{GAS}.RPM}{T_0.P_0.10^5} \quad (2)$$

Where,

P_{gas} (bar) = Actual pressure of the gas

V_{gas} (cm^3) = Cumulative gas volume into the pre-chamber per cycle

T_{gas} (K) = Actual temperature of the gas

RPM = Revolutions per minute

T_0(K) = Standard temperature

P_0 (bar) = Standard pressure

To vary the GR pressure during the simulation to get the required gas flow rate, a PID controller was added to the model. The PID controller works with the following equations (3) (4) (5).

$$\frac{dx_1}{dt} = u \quad (3)$$

$$\frac{dx_2}{dt} = \frac{u - x_2}{t} \quad (4)$$

$$y = \left(K_P + \frac{K_D}{t}\right)u + K_I x_1 - \frac{K_D x_2}{t} \quad (5)$$

Where 'K_P' is the proportional gain, 'K_I' is the integral gain, 'K_D' is the derivative Gain, 't' is the derivative time constant, 'y' is the controller output, 'u' is the difference between the reference signal value and the input signal value and 'x_1' and 'x_2' are the initial state variables [13].

For the gas flow rate PID controller, the controller output is the gas pressure value and the target for the input signal (reference signal) is the required gas flow rate value which is given by the user at the start of the simulation. The input signal value is developed by an RLT sensor. The RLT sensor gives the output developed by the equation (6). The cumulative gas volume into the pre-chamber per cycle for the equation is given by an integrator function implemented in the model. The proportional gain, integral gain and Derivative gain was manipulated to get steady output value close to the required value in a short time according to the manual in [13]. The final values for proportional, integral gain and derivative gain are 0.1, 0.12 and 0.

The simulation is performed again with gas flow rate PID controller with the case setup in the Table 5 with one additional case setup input "gas flow rate required" which was set to a value of 0.2m^3/h. The Figure 22 shows a plot of GR pressure and the gas flow rate for different engine speeds. From the Figure 22 we can observe that the gas flow rate PID controller is working properly as the GR pressure is continuously changed by the PID controller to maintain the required gas flow rate into the pre-chamber for different engine speeds.

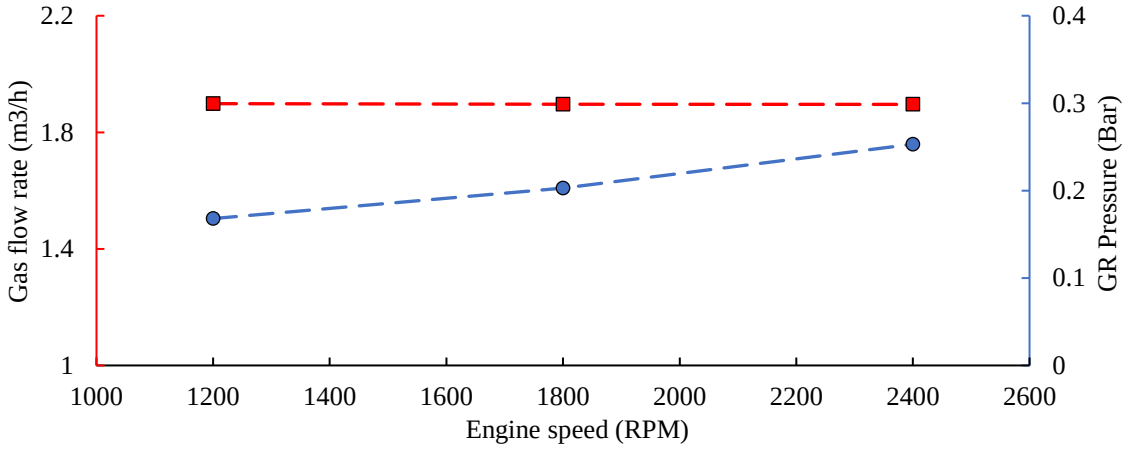

Figure 22 Plot of GR pressure and the gas flow rate into the pre-chamber for different engine speeds

5.2.2 Exhaust lambda controller

The Lambda in the exhaust must be controllable by the user in the model. In the above simulation, we can see that the cumulative gas volume per cycle is not the same in various engine speeds. When the lambda in the intake is kept at 1 and additional gas is added into the pre-chamber, the fuel mixture becomes richer. As the cumulative gas volume into the pre-chamber per cycle changes with engine speed, the lambda in the exhaust is not constant in various engine speed which can be observed in the Figure 23.

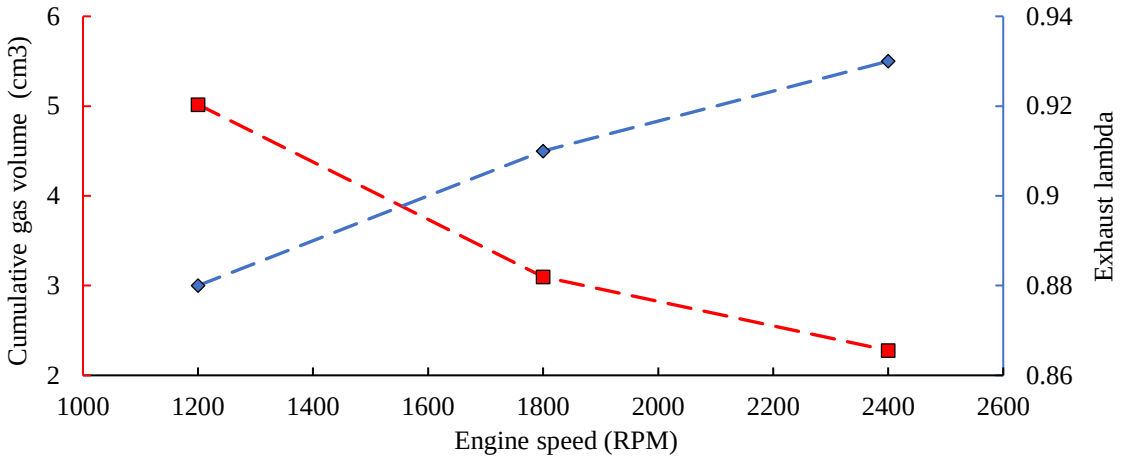

Figure 23 Cumulative gas volume per cycle and the lambda in the exhaust for various engine speeds

To control the lambda in the exhaust, an exhaust lambda *PID* controller was added which worked on the equations (3)(4)(5). The proportional gain, integral gain and Derivative gain was manipulated to get steady output value close to the required value in a short time according to the manual in [13]. The final values for proportional, integral gain and derivative gain are 0.3, 0.2 and 0. The controller output was fuel air ratio to injector in the intake, the target for the input signal (reference signal) is the required exhaust lambda which is given by the user at the start of the simulation. The input signal value is developed by the moving area function implemented in the model that takes the average of the Lambda in the exhaust per cycle. The lambda *PID* controller changes the lambda in the intake by changing the fuel flow in injector to get the required exhaust lambda. The case setup parameter 'intake lambda' is not required anymore, a. The case setup has new parameter 'exhaust lambda' which must be set by the user according to the required value.

5.2.3 MEP controller

If the Engine must be tested in different load conditions either the throttle angle or the MEP (mean effective pressure) must be changed. If the throttling is increased the volumetric gas flow into the main chamber increases. Therefore, MEP and throttling are related by the equation (6) [9].

$$\mathrm{MEP} = \eta_v \eta_f Q_{hv} \rho_{a,i} \frac{F}{A} \tag{6}$$

Where, η_v is the volumetric efficiency, η_f is the fuel conversion efficiency, Q_{hv} is the heating value of the fuel, $\rho_{a,i}$ is the density of the inlet mixture and $\frac{F}{A}$ is the fuel air ratio.

In the case setup of the model the throttle position can be changed by the user. The model should be simulated several times to operate the engine in the demanded MEP by changing the throttle angle manually. To avoid this long process a MEP PID controller with an on/off switch was incorporated which works on the principle equations (3)(4)(5). The proportional gain, integral gain and Derivative gain was manipulated to get steady output value close to the required value in a short time according to the manual in [13]. The final values for proportional, integral gain and derivative gain are 1, 1.2 and 0. The controller output is the throttle angle, the target for the input signal (reference signal) is the demanded MEP which is given by the user at the start of the simulation. The input signal value is developed by the RLT sensor which gives the MEP of the cylinder. There is on/off switch installed so that it can be controlled by the user whether the MEP PID controller should be used or not. There are 2 additional case setup parameters, one is 'MEP controller switch' to switch the controller on - 1 or off - 0 and the second 'Demanded MEP' to specify the Required MEP. If the controller is on, the 'Demanded MEP' must be set by the user and the throttle angle set by the user is of no use. As the MEP PID controller will alter the throttle angle to get the required MEP. If the controller is off, the demanded MEP need not be specified by the user. Instead the throttle angle must be set.

5.2.4 EGR controller

The EGR (exhaust gas recirculation) is a technique to control the SI engine knocking. The main reason for knocking is high temperature in the combustion chamber. The peak temperature is reduced by adding a fraction of exhaust gases to the engine intake system. This Exhaust gas act as a diluent to the intake mixture and reduces the peak temperature. One another benefit of EGR is reduction in NO_x emissions which is again caused by high peak temperatures in the chamber. To control the EGR in the model, a Controller EGR valve was implemented in the model. The controller EGR valve regulates the EGR by controlling the orifice diameter of the EGR connection. The desired EGR is given as an input by the user. It controls the throttling or orifice diameter of the EGR correction according to the EGR present in the intake system until the target EGR specified is reached. The case setup has an additional parameter added – 'EGR'.

5.3 Model calibration and comparison

The experimental data from the single cylinder pre-chamber engine was given by the consultant to Calibrate the model. The data was for constant engine speed of 1800 RPM and was for 3 different lambdas 1.048, 1.542, 1.994 with fully open throttle. The combustion model in the GT-POWER model is not same as the experimental engine. Some data like burn rate, residual fraction, trapping ration cannot be measured directly in the experimental model. So, to get the data from the experimental engine regarding the combustion model, TPA (Three pressure analysis) method was performed by the predecessors. To extract the data from the experimental setup a TPA model was created in the GT-POWER like the experimental setup and the experimental pressure data and heat release data from the experimental engine was given as an input. Reverse cycle analysis was done to calculate the burn rate. This step was iterated to get a steady value [15]. The combustion model extracted from the experimental engine was given as an input in the created model. The Figure 24 shows a plot between CA10-90 for pre-chamber and the main chamber vs exhaust lambda. The CA50 for the main chamber is 10 degrees and for the pre-chamber, it can be seen in the table 6. The Wiebe exponent for the main chamber and the pre-chamber are 1 and 1.5. The input of CA10-90 for main chamber is

given as a XYZ map in the model. The Figure 25 shows the plot between the burned fraction of the fuel and the exhaust lambda in the combustion model.

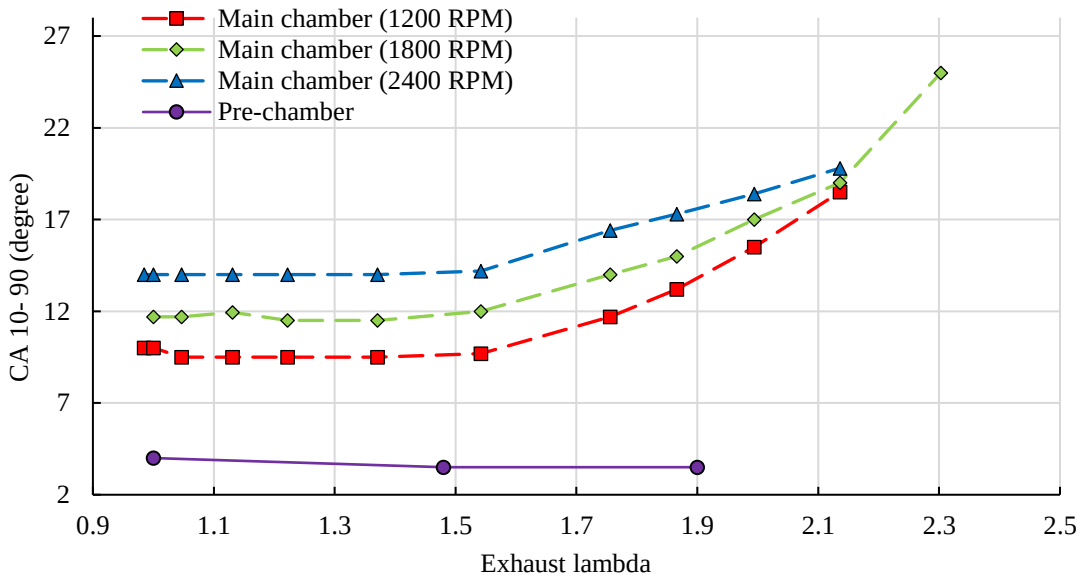

Figure 24 Plot between CA10-90 and exhaust lambda for different engine speeds

Lambda	CA50 (Degree)
1	-1.3
1.48	-2.4
1.9	-6.5

Table 6 CA50 for various operating lambda in the pre-chamber combustion model

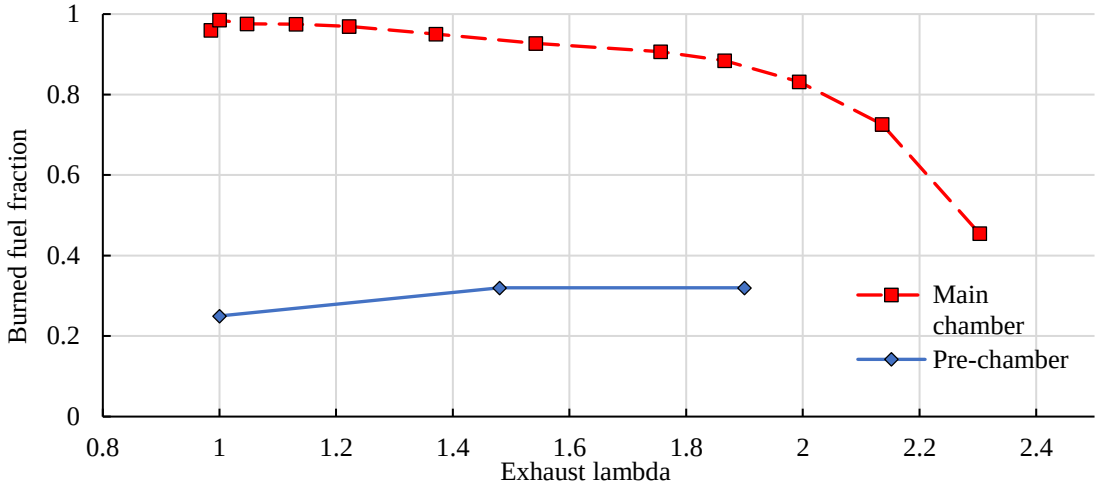

Figure 25 Plot between the burned fraction of the fuel and the exhaust lambda in the combustion model

The model was operated with same parameters as that of the experimental engine. The model was simulated with 1800 RPM in different lambda. The throttle is fully open in the experimental data. But, if the throttle is fully open in the model the MEP will be much higher in the model than in the experimental data, as experimental data is from a single cylinder engine and the created model is a 4-cylinder engine [9]. So, the MEP of the

experimental data for different lambda was given as the ‘demanded MEP’ to simulate the same load conditions in the created model. Three different cases were simulated, case 1 with Exhaust lambda 1.048 and MEP 10.18 bar, case 2 with exhaust lambda 1.542 and MEP 7.3 bar and case 3 with exhaust lambda 1.994 and MEP 5.75 bar. Main parameters of the case setup for model comparison simulation is listed in the Table 7.

Parameter	Unit	value
MEP controller switch’		1(on)
Demanded MEP	Bar	10.18, 7.3, 5.75
Exhaust Lambda		1.048, 1.542, 1.994
Gas flow rate required	m^3/h	0.3
Engine speed	RPM	1800
Turbine rack position		1 (no boost)

Table 7 Main parameters of the case setup for model comparison simulation

The Figure 26 is a plot of the main chamber pressure against the crank angle for the case 1. It can be observed that the maximum main chamber pressure for experimental data is than less than in the model, i.e. 60.48 bar and 62.38 bar respectively. The maximum difference in main chamber pressure along the crank angle can be seen only at peak pressure points. When the engine is operated at lambda 1.048 the maximum pressure difference between the model and the experimental data is 1.9 bar which is around 3%, which is comparable considering it occurs only at the peak point. The Figure 27 shows a plot of the main chamber pressure against the crank angle for case 2. It can be observed that the maximum main chamber pressure for experimental data is less than that of the model, which are 47.9 bar and 52.14 bar. Same as the previous case, the maximum difference in main chamber pressure along the crank angle can be observed only at peak pressure points. When the engine is operated at lambda 1.542 the maximum pressure difference between the model and the experimental data is 4.24 bar which is around 9%, which is 3 times more difference that was calculated in case 1. The Figure 28 shows a plot of the main chamber pressure against the crank angle for case 2. It can be observed in case 3 that the maximum main chamber pressure for experimental data is less than that of the model, which are 38.48 bar and 40.68 bar respectively. Like above cases, the maximum difference in main chamber pressure along the crank angle can be observed only at peak pressure points. When the engine is operated at lambda 1.994 the maximum pressure difference between the model and the experimental data is 2.2 bar which is around 6 %, which is lower than case 3 and higher than case 1.

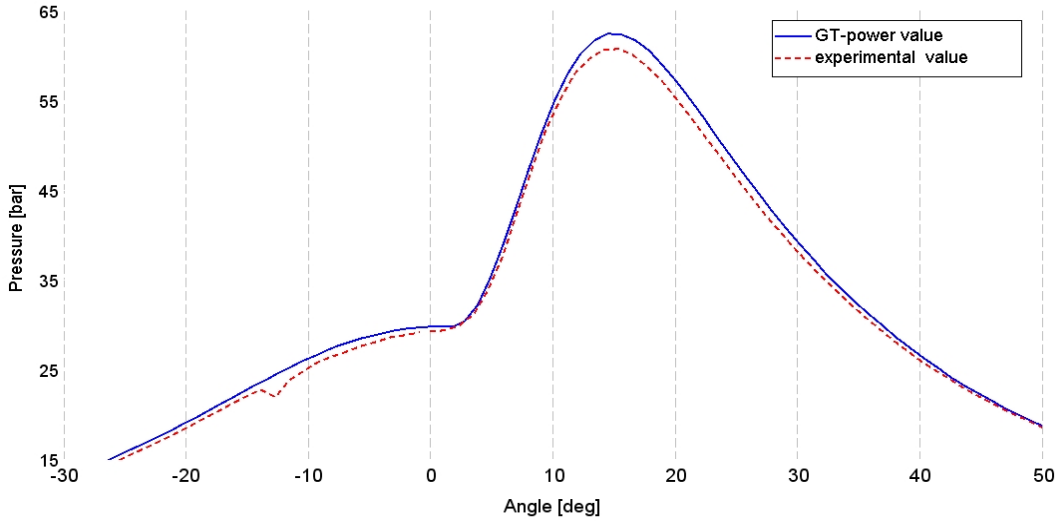

Figure 26 Plot of the main chamber pressure against the crank angle for Exhaust lambda 1.048 and MEP 10.18 bar

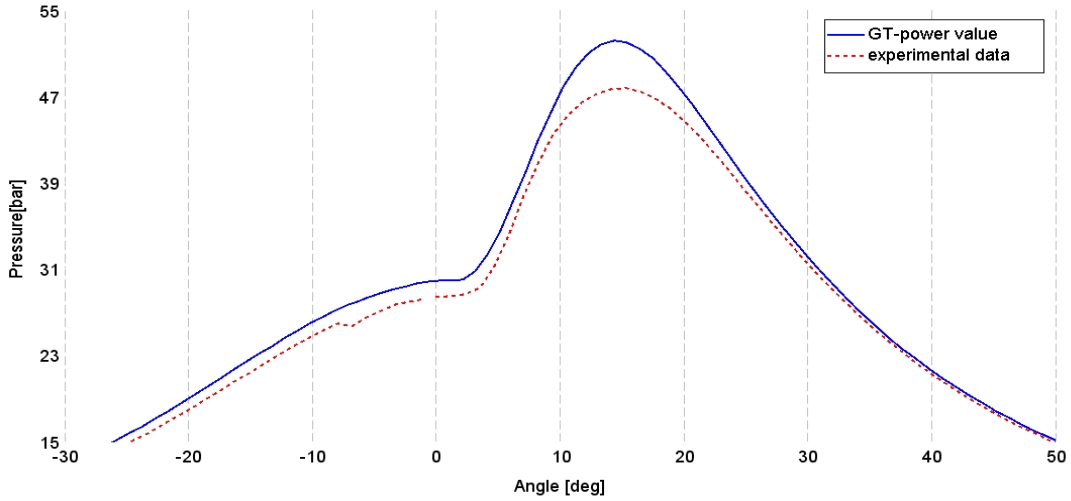

Figure 27 plot of the main chamber pressure against the crank angle for exhaust lambda 1.542 and MEP 7.3 bar

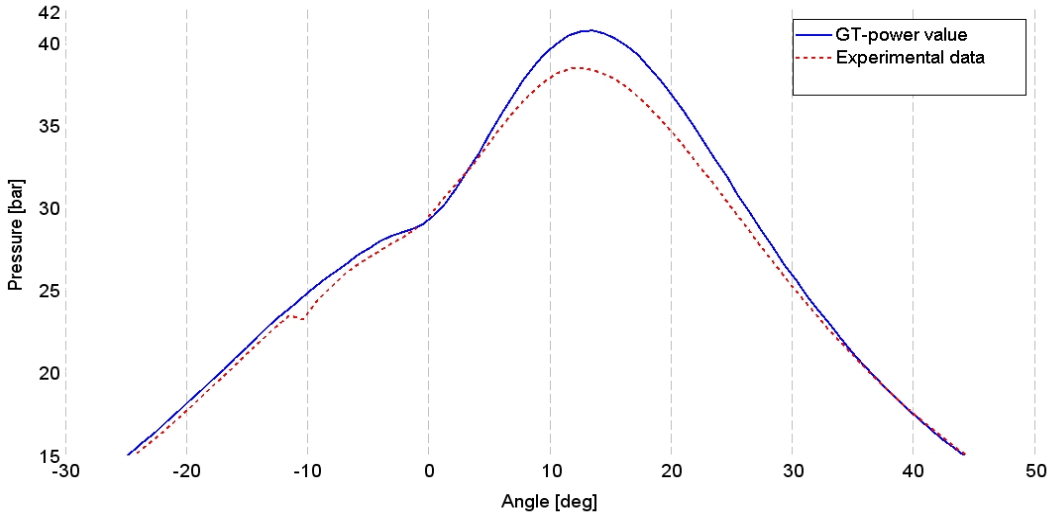

Figure 28 plot of the main chamber pressure against the crank angle for exhaust lambda 1.994 and MEP 5.75 bar

Some variations are observed in the peak pressures in all the cases. The variations in the peak pressure is not because of the variations lambda and MEP because variations were observed to be less than 0.3 percent, which will not cause any noticeable changes in the peak pressures. When the combustion model was examined it was evident that there was some considerable difference between the model and experimental engine. Figure 29 presents a plot of the CA50 and CA-10-90 against exhaust lambdas. The CA50 which gives information about the start of combustion and CA10-90 shows the burned duration. These influence the peak pressure and the angle at which the peak pressure occurs [9]. The model is created with main and pre-chamber combustion model separately. Both the chambers are not considered closed by the GT-POWER. So, during combustion the specific combustion model assigned for the chambers influence one another causing the variations in CA-50 and CA10-90. The cylinder to cylinder peak pressure variations was also observed. The table 9 compares the main chamber pressure in each cylinder against crank angle for case 1, 2 and 3. From the table 8, it was observed the cylinder to cylinder pressure variations are within 0.3 percent change in all the cases. From the magnitude of the variations in cylinder peak pressure and the pressure difference between the model and experimental data, the created model was considered optimally calibrated for further proceedings.

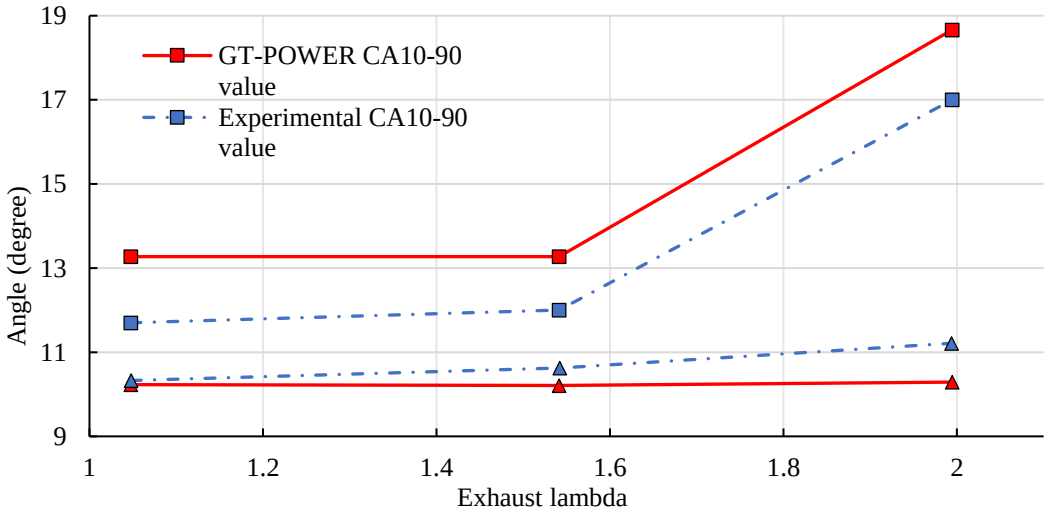

Figure 29 Plot of the CA50 and CA-10-90 in main chamber against exhaust lambda

	Cylinder 1 peak pressure (bar)	Cylinder 2 peak pressure (bar)	Cylinder 4 peak pressure (bar)	Cylinder 4 peak pressure (bar)	Cylinder to cylinder peak pressure variation (%)
Case 1	62.38	62.72	62.877	62.55	0.26
Case 2	52.138	52.138	52.305	52.14	0.15
Case 3	40.68	40.71	40.75	40.67	0.06

Table 8 Peak pressure in the cylinders and the cylinder to cylinder peak pressure variation in each operating case

5.4 Full load model simulation and comparison

Based on the results from the simulations in previous section, the model is well calibrated with the experimental engine. Since the model created represents a 4-cylinder setup, it would be pointless to compare the, torque, turbine, compressor, intake and exhaust properties with part load conditions. As the MEP controller was used in the previous simulation, the model's full load operation wasn't tested. There is a lot of pressure, temperature and flow difference in full, part and low load conditions in an engine [11]. We get the maximum torque and power output form the engine in full load condition, this can be considered as the extreme operating case of the engine. To test the working of the designed GR, it is recommended to simulate the engine in the full load condition because the temperatures, pressures and flow will be in a much higher order when compared to part load or low load conditions. The aim of this section to Calculate the full load characteristics of the model while considering the physical limitations of the components in the experimental setup and comparing it with the experimental data from a 4-cylinder original SI engine. The performance map of the model is plotted in this section.

5.4.1 Full load simulation of the model

In the future, when the experimental engine is converted to 4-cylinder engine with pre-chamber like the model setup, the parts in experimental setup will experience much higher physical loads like high pressure, temperature, flow etc than the present experimental setup. The working parts of laboratory engine setup has some physical limits which must be taken into consideration when simulating the full load curves for the model. The experimental engine can withstand a maximum cylinder pressure of 120 bar. The Turbo

charger will withstand speed up to 160000 RPM. The exhaust temperature before the turbine has a limitation of 800 C.

The VGT turbocharger is used in the experimental engine. The VGT helps to alter the turbocharger RPM for same engine speed and give a high compressor boost pressure. The VGT turbo charger has rack position from 0 to 1. The position 0 gives the maximum compressor boost pressure and 1 gives no compressor boost pressure. The model was simulated in the full load condition by switching off the MEP controller and the throttle angle in fully open position. It is well known that the torque output of the engine is greater when operated in maximum compressor boost pressure. When the compressor boost pressure is maximum, the amount of air/fuel mixture going inside the engine is more compared to the amount at no compressor boost pressure condition. If the amount of air/fuel mixture going inside engine increases, the volumetric efficiency of the engine increases which gives more torque /power output [9].

The first set of simulations were performed with the following case setup parameters shown in the table 9 to calculate the full load curve. The combustion models for the main chamber and the pre-chamber were not changed from the previous simulation. The full load simulation was performed with no additional gas supply to the pre-chamber, that is the pre-chamber was not scavenged. The VGT rack position was tuned manually to produce maximum torque possible within the physical barrier limits.

Parameter	Unit	value
PID switch		0(off)
Throttle angle	degree	90 (full open)
Exhaust Lambda		1
Gas flow rate required	m^3/h	0
Engine speed	RPM	800-2600

Table 9 case setup parameters for full load simulation and comparison

From the first set of simulations, the torque of the model was observed to be less in low engine speeds when compared to 4-cylinder original SI engine. However, the torque of the model increases more than the 4-cylinder original SI engine engine when high engine speeds are reached. The above phenomenon is absurd as the torque output of the model must be more or closer to the data from the 4-cylinder engine original SI engine because when the combustion stability is better in pre-chamber engine, it gives more engine efficiency [15]. When the data of the simulation value and experimental data were

Examined it was found that some parameters of the model and the 4-cylinder original SI engine were not comparable. It is observed that the Turbocharger speed of the model is lesser than the 4-cylinder original SI engine in all engine speed. Eventually, the intake pressure was lesser than the original engine. At constant engine speed and VGT position, the turbocharger speed depends on the mass flow rate of the exhaust gases through the turbine. There was a decrease in exhaust temperature in the model when compared to the original engine, which was the reason for the drop in the turbocharger speed. As it is clear that when the exhaust temperature is high, there is higher mass flow rate [11]. All the above results conclude to the point that the combustion model used in the simulation is not optimum for giving the maximum output.

The second set of simulations was performed to find the optimum combustion timing and duration to produce maximum output. The combustion duration was doubled as it was noticeably short when compared to the typical values [13]. CA50 of the main chamber was simulated from 15 to 30 degrees with a step of 2.5 to find at which CA50 the model is producing the highest torque. During the combustion phasing analysis, the VGT rack position was tuned manually to produce maximum output possible within the physical barrier limits. Even when there was no compressor boost pressure, the physical limits were crossed at certain CA50. So, the throttle angle was tuned manually to keep the values within the physical barrier limits of the components. From the results of the second simulation, there was an increase in the torque output at lower engine speeds when compared to the first set of simulations. At higher engine speeds the engine performance was poor when compared to the first simulations data. When the VGT rack position and the throttle angle was tuned to control the exhaust temperature and turbocharger speed from reaching its limits at higher engine speeds, there was a drastic drop in the torque output of the engine. The throttle angle tuning to reduce exhaust temperature had a larger negative effect in the torque output.

To control the exhaust temperature and the turbocharger speed from the crossing the limits EGR was used with VGT rack position tuning instead of Throttle angle control in the third set of simulation. The combustion timing sweep part of the simulation was kept same as that of the second simulations. From the result it was evident that the EGR tuning is better than throttle angle tuning for controlling the exhaust temperature without drastically affecting the torque output. All the physical component parameter values where under the limit with better torque outputs when compared to the simulations using

throttle angle tuning instead of EGR tuning. From the figures 30, 31, 32 and 33 we can notice that engine setup's physical limits were not crossed. From the engine speeds 1400 to 1800 RPM the tuning was mainly to control the Exhaust temperature and the Turbocharger speed from crossing the limit. From engine speed of 1800 to 1600 RPM the tuning was mainly to control the Turbocharger speed and the maximum power limitation of the engine from crossing the limit.

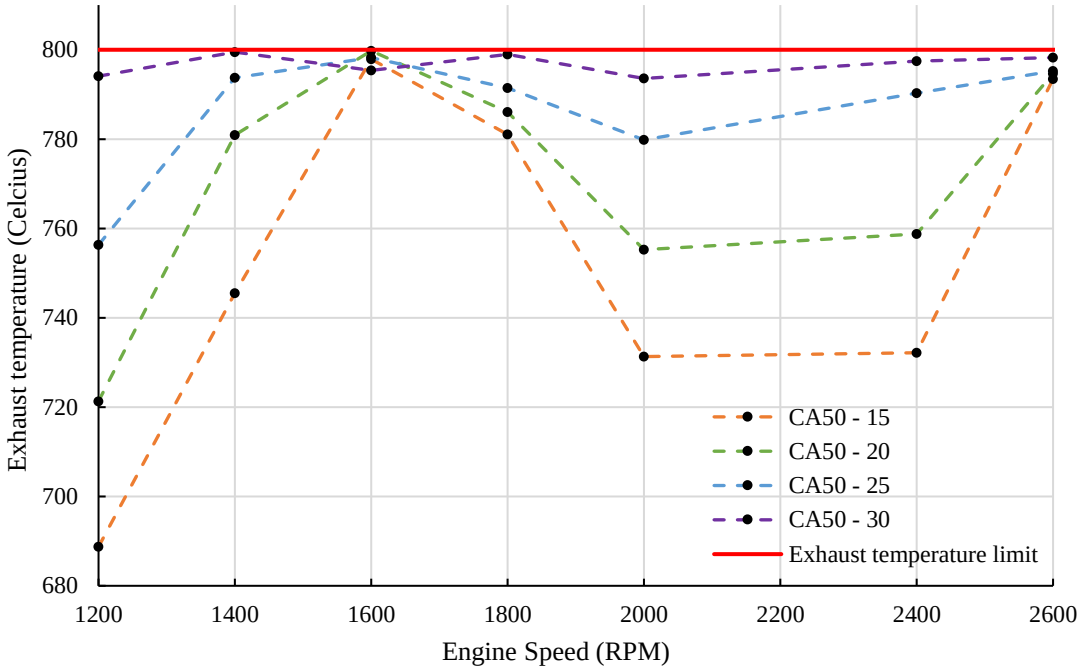

Figure 30 Exhaust temperature vs the engine speed for different CA50(degree)

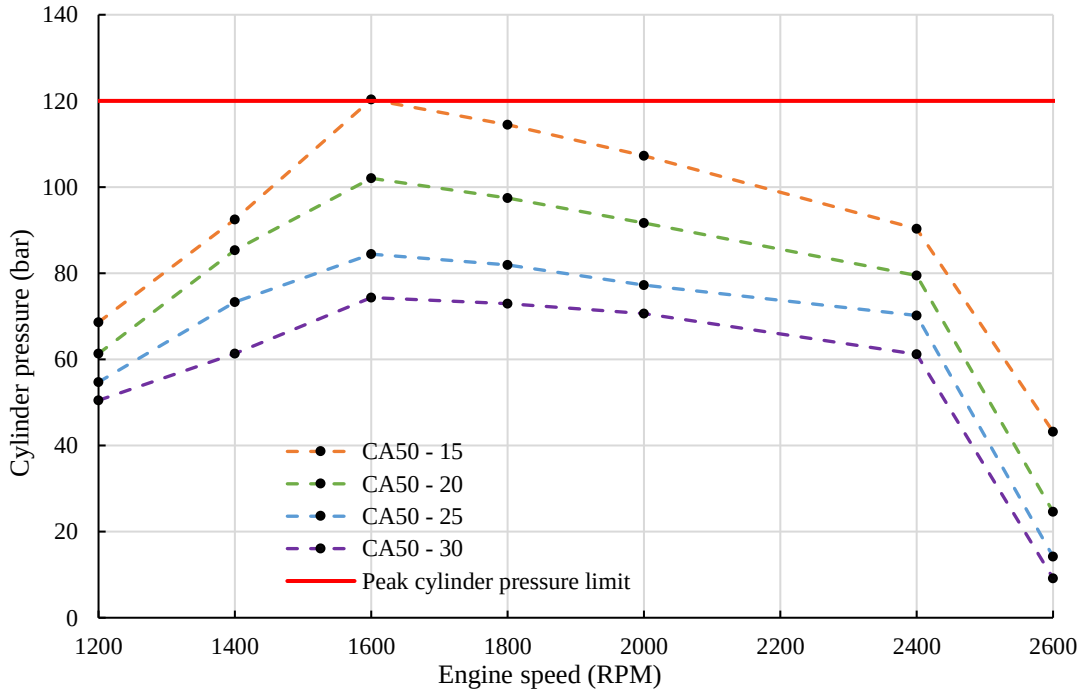

Figure 31 Cylinder pressure vs the engine speed for different CA50(degree)

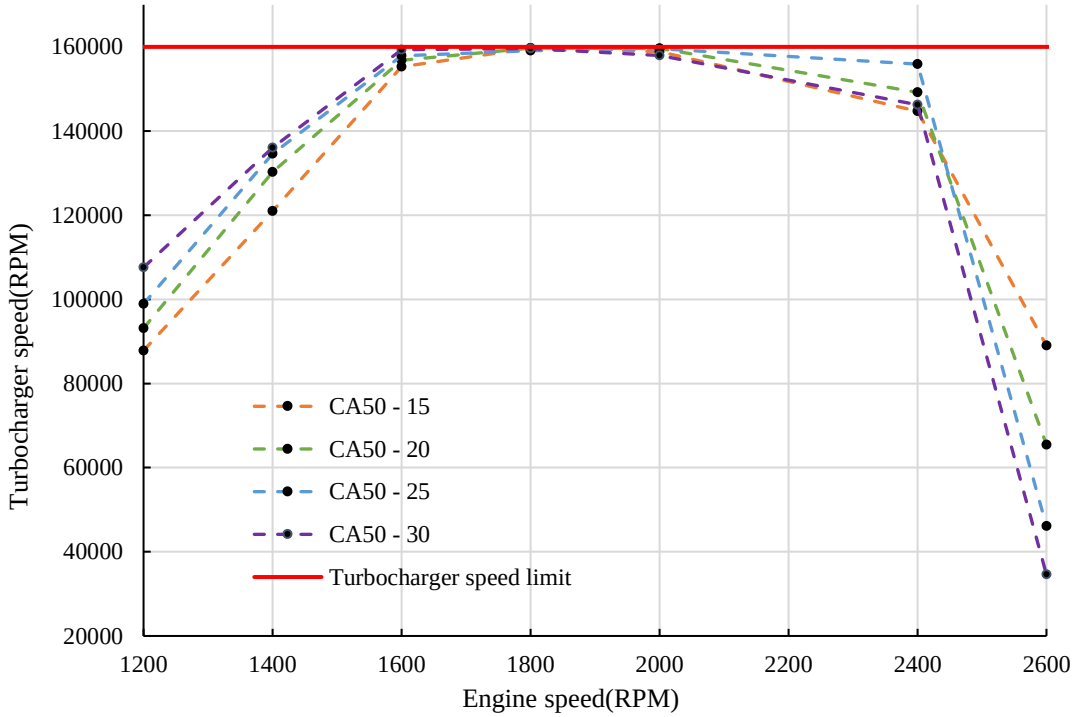

Figure 32 Turbocharger speed vs engine speed for different CA50(degree)

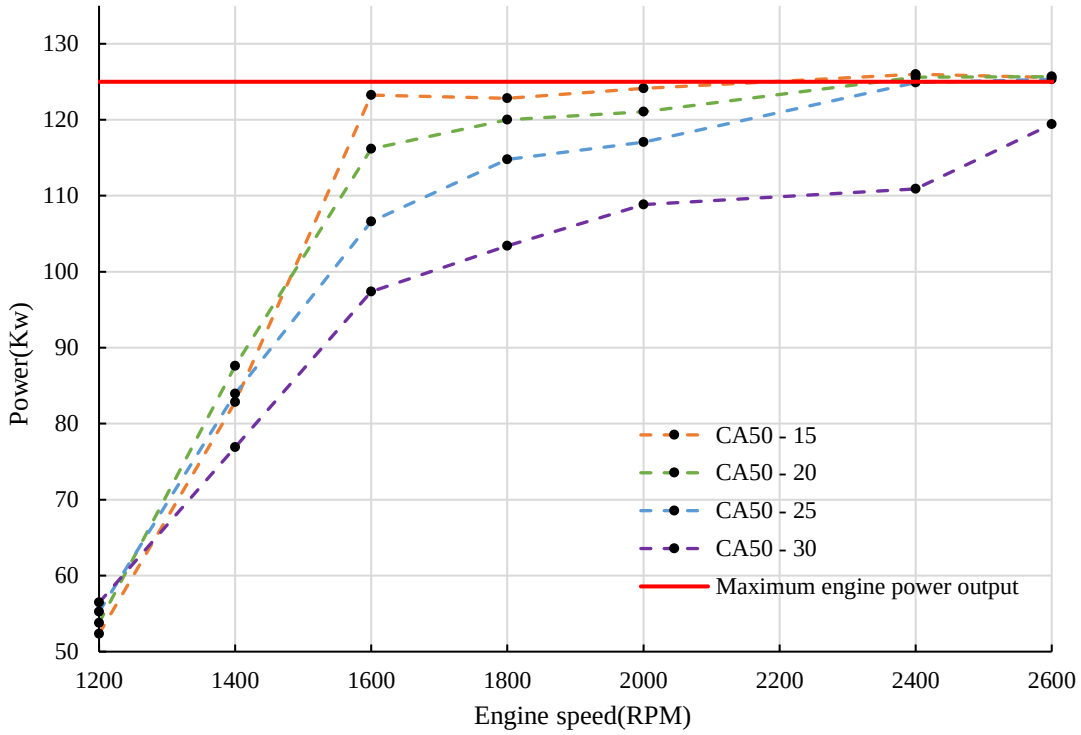

Figure 33 Power vs engine speed for different CA50(degree)

The data from the simulations were compared with the experimental data from a 4-cylinder original SI engine. From the results, we conclude that CA50-25 degree is the optimum timing to get maximum performance without crossing the limits. At CA50-25 degree, the model performs better than the original engine at all engine speeds tested. At

all other CA50 readings there is at least one place where the engine torque output goes below the original 4-cylinder SI engine. The table 10 shows the torque and engine speed readings for different CA50. When the torque produced by the engine at a certain speed and CA50 goes below the torque of the original 4-cylinder SI engine, it is highlighted with red marking. From the table seen that at CA50 – 25 degree there is no drop in the torque below the original engine's value. If 1.5 percent drop in the torque when compared the original engine is tolerable, then CA50-22.5 degree is considered optimum as it has higher torque values at high engine speeds when compared to CA50 – 25 degrees. Figure 34 shows the torque for different CA50. Table 11 shows the VGT rack position and EGR percentage for different CA50.

Torque (N-M)	**CA-50(degree)**						
Engine speed (RPM)	15	17.5	20	22.5	25	27.5	30
1200	416.6	423.17	428.18	431.38	439.83	442.00	449.40
1400	565.3	582.48	597.68	612.05	572.72	554.05	524.85
1600	735.8	720.86	693.60	652.29	636.49	606.24	581.52
1800	651.8	647.35	636.98	626.48	609.14	577.06	548.80
2000	592.9	587.56	578.22	568.6479	559.11	541.76	519.98
2400	501.5	500.51	500.06	497.80	497.2	486.8	441.54
2600	461.8	461.48	461.78	461.69	460.53	454.60	438.8

Table 10 Torque, engine speed readings for different CA50 with values of torque marked in red where it goes below the torque values of original4 cylinder SI engine.

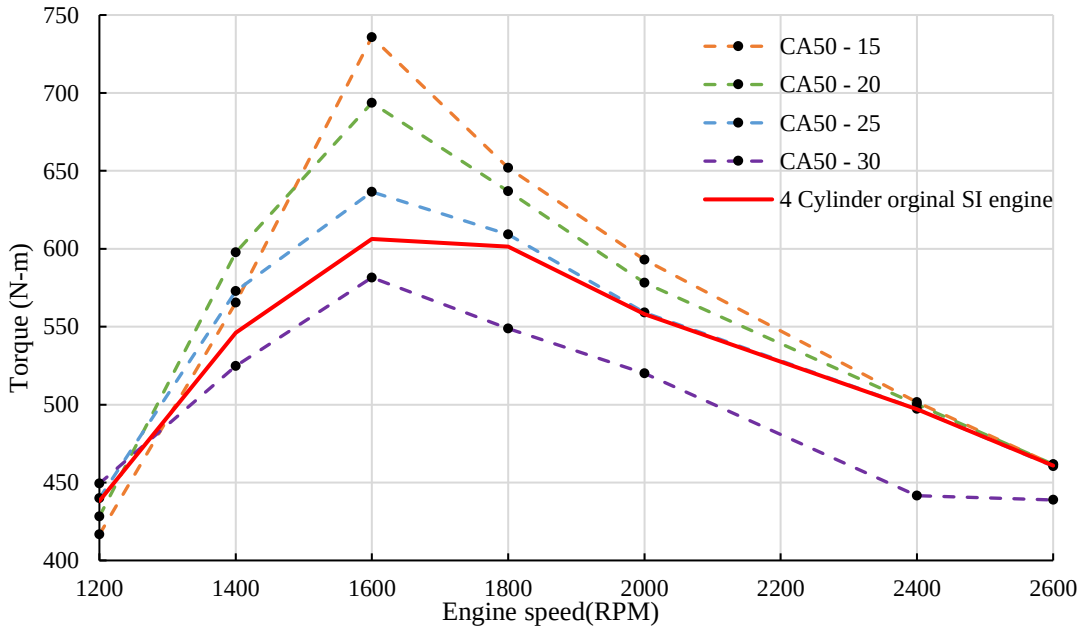

Figure 34 Torque vs engine speed for different CA50(RPM)

Engine speed (RPM)		CA-50(Degree)						
		15	17.5	20	22.5	25	27.5	30
1200	VGT position	0	0	0	0	0	0	0
	EGR (%)	0	0	0	0	0	0	0
1400	VGT position	0	0	0	0	0	0	0
	EGR (%)	0	0	0	0	3.9	5.6	7.5
1600	VGT position	0	0	0	0	0	0	0
	EGR (%)	1	2.8	5	7.8	9	10.9	12.4
1800	VGT position	0.05	0.16	0.27	0.37	0.43	0.43	0.43
	EGR (%)	9.8	10	10.6	10.8	11	12.8	14.2
2000	VGT position	0.42	0.44	0.46	0.49	0.52	0.55	0.6
	EGR (%)	15	15	15	15	15	15	15
2400	VGT position	0.83	0.84	0.84	0.84	0.82	0.81	1
	EGR (%)	16	16	16	16	16	16	16
2600	VGT position	1	1	1	1	1	1	1
	EGR (%)	20	20	20	20	20	20	20

Table 11 VGT rack position and throttle angle for different CA50 at different engine speed with the optimum CA50 setting highlighted in yellow.

5.4.2 Performance map of the model

The model was set with an optimum CA50-25 degree in all the following simulations. The full load simulation was performed with no additional gas supply to the pre-chamber. The model was simulated with tuned EGR and VGT setting for maximum torque output with the parameters of the components under the limit. The EGR and VGT setting for maximum torque is given below in table 12.

The model was also simulated with constant EGR. For the constant EGR setting, the VGT and throttle angle setting were tuned to keep the values of exhaust temperature, peak cylinder pressure and turbocharger speed within limits. First, the VGT rack setting was tuned to bring down the turbocharger speed and exhaust temperature under the limit. Some engine speeds still had exhaust temperature going over the limit, this was controlled by throttle angle setting. The throttle angle and VGT setting for constant EGR operation is given below in table 13. From the simulation, it was observed that torque output of constant EGR operation setting was lower than that of the tuned EGR setting. This was because at constant EGR operation setting, the throttle angle was reduced to control the exhaust temperature. Reduction of throttle angle leads to lowering of the torque output. Whereas in the Tuned EGR setting the use of throttle angle reduction is not necessary as physical parameter values where under the limit. Performance map of the Model with CA50 – 25degree is shown in figure 35.

Engine speed (RPM)	1200	1400	1600	1800	2000	2400	2600
VGT position	0	0	0	0.43	0.52	0.82	1
EGR (%)	0	3.9	9	11	15	16	20

Table 12 The EGR and VGT setting for maximum torque output

Engine speed (RPM)		EGR (%)			
		3	9	11	15
1200	VGT position	-	-	-	-
	Throttle angle (degree)	-	-	-	-
1400	VGT position	0.05	-	-	-
	Throttle angle (degree)	90	-	-	-
1600	VGT position	0.6	0	-	-
	Throttle angle (degree)	90	90	-	-
1800	VGT position	1	0.6	0.43	-
	Throttle angle (degree)	90	90	90	-
2000	VGT position	1	0.9	0.8	0.55
	Throttle angle (degree)	8	90	90	90
2400	VGT position	1	1	0.84	0.85
	Throttle angle (degree)	5	8	16	90
2600	VGT position	1	1	1	1
	Throttle angle (degree)	4.5	15	20	20

Table 13 The throttle angle and VGT setting for constant EGR operation.

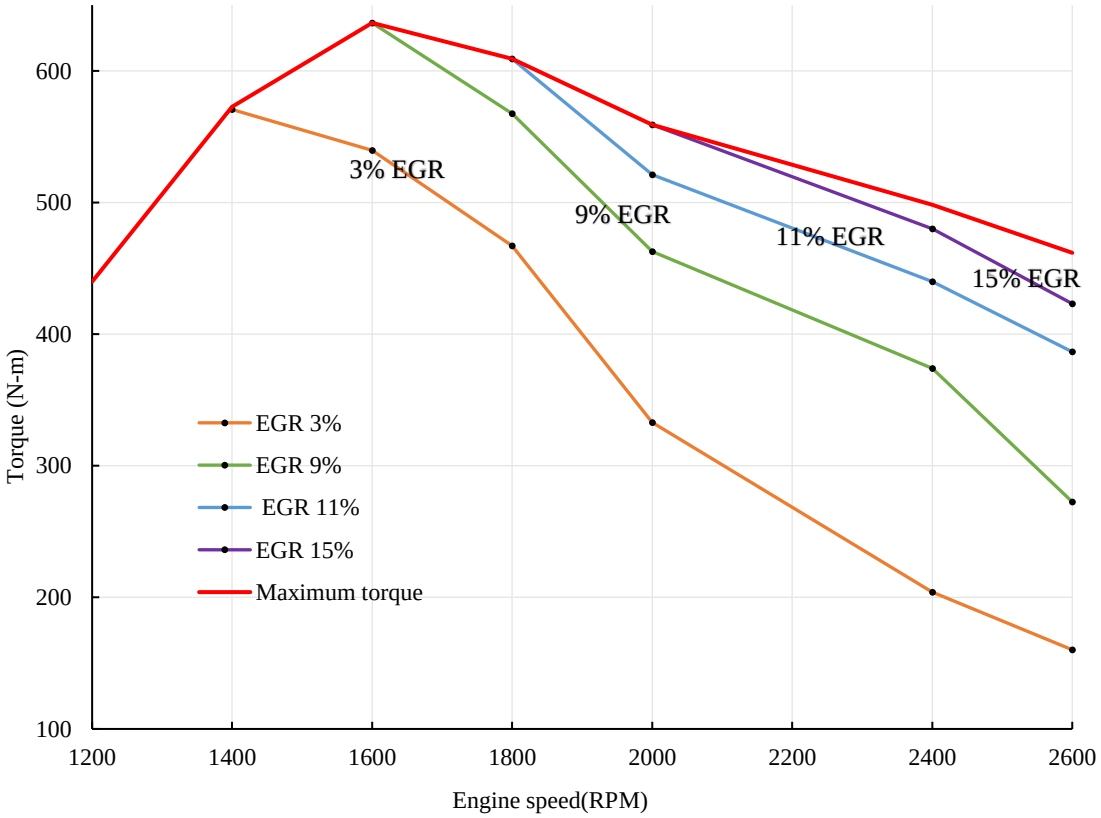

Figure 35 Performance map of the Model

When the data from the simulations and the data from the experiments of 4-cylinder original SI engine was compared, it was noted that the BSFC of the model was more at tested engine speeds. It was concluded that, even though the CA50-25 degrees setting of the model brings out the maximum torque output, it was not the optimum setting in terms of the BSFC values. The performance of the Model was better than the 4-cylinder original SI engine in terms of the torque output but not in terms of BSFC. The CA50 must be further optimized to find the optimum CA50 value in terms of both torque output and BSFC. Figure 36 shows the comparison between the model and the 4-cylinder original SI engine.

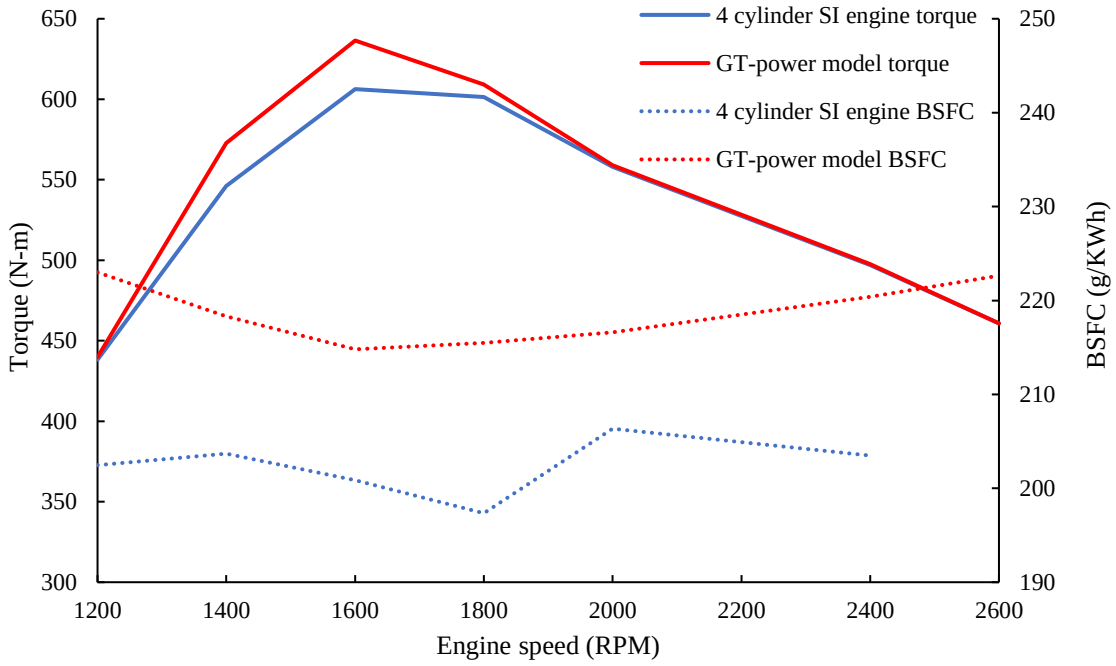

Figure 36 the comparison between the model and the 4-cylinder original SI engine.

Chapter 6 Gas rail

6.1 Effect of scavenging pre-chamber

All the previous simulations in chapter 5 were conducted without pre-chamber scavenging. Simulations were performed to study the effects of scavenging the pre-chamber. The model was simulated using various gas flow rate setting to observe effect of various scavenging percentages. The lambda exhaust was kept constant at 1. The model was simulated at an engine speed of 1200RPM.The CA50 of the model was set at 25 degrees for all following simulations.

The effect of increasing scavenging on the lambda in the pre-chamber during the time of spark and in the main chamber is shown in the figure 37. It is evident that if the scavenging is increased, the lambda in the pre-chamber during the time of spark increases. The lambda in the main chamber increases when the scavenging is increased. It can be concluded that if the pre-chamber is scavenged, it enables operation of engine with leaner mixture

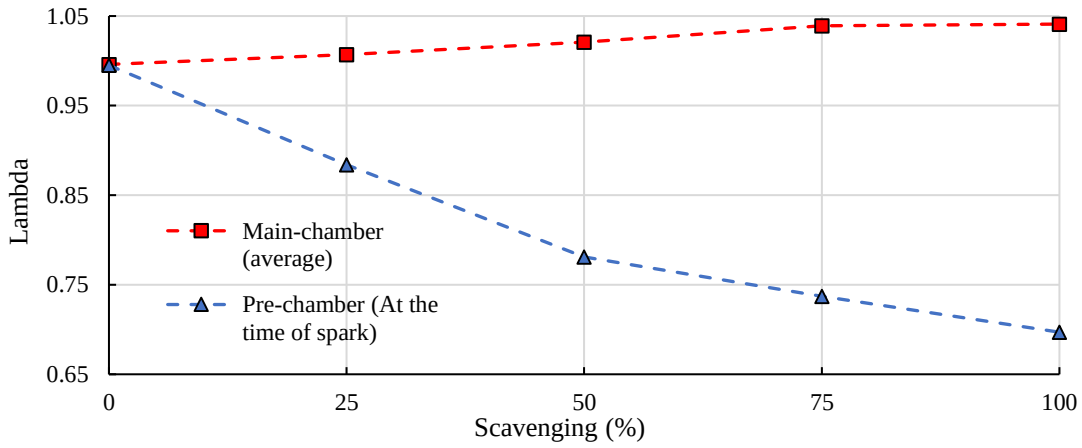

Figure 37 Influence of scavenging on lambda

When the Pre-chamber is scavenged the amount of unburned fuel increases which calculated in terms of HC emissions. As there is very rich mixture during at the time of spark, the combustion efficiency in the pre-chamber goes down when pre-chamber is scavenged. But, as pre-chamber is an ignition system for the main chamber. The energy

created by the pre-chamber is a much more important parameter. The energy created by the pre-chamber was calculated from the combustion efficiency and the fuel energy entering the pre-chamber. It can be seen from the table 14 that the energy created by the pre-chamber is more when it is scavenged. It is also noticed that scavenging the pre-chamber reduces the temperature in the pre-chamber and main chamber.

Scavenging (%)	0	25	50	75	100
Specific HC emission (g/kW-h)	5.14	5.7	6.5	6.76	7.5
Combustion efficiency in the pre-chamber (%)	24.8	22.6	20.07	19.17	18.9
Fuel energy entering the pre-chamber (J)	50.7	58.9	65.4	70.7	70.8
Energy released by pre-chamber (J)	12.57	13.31	13.73	13.43	13.58
Maximum temperature in the pre-chamber (Celsius)	1148	1128	1106	1091	1087

Table 14 Effects of scavenging of pre-chamber on the model.

Scavenging the pre-chamber helps to remove a lot of heat and reducing the thermal stress. High temperature may cause pre-ignition hence making the combustion unstable. The main chamber operates in leaner mixture when the pre-chamber is scavenged. The ignition energy produced by the pre-chamber in the main chamber was greater when the pre-chamber was scavenged.

6.2 Gas rail performance analysis

6.2.1 Discretization length setting

The Discretization length is the length into which the GR will be subdivided for the calculations in the GT-power software. A discretization length of 10mm to 20mm is usually recommended for the modelling a fuel intake system [13]. Smaller discretization lengths should be used to get higher resolution in the results and will take much longer simulation time. For systems that doesn't need much accuracy and needs faster run times, larger discretization length is used. The model was simulated in full load condition at an engine speed of 1800 RPM for discretization lengths of 10mm, 15mm and 20mm respectively. The additional gas was supplied to the pre-chamber So as to test the resolution of GR datas for different discretization length. The simulation gas flow rate was set to $0.3m^3/h$ and the exhaust lambda was set to 1.

From the simulation it was noted that there was a fall in the cumulative gas flow into the pre-chamber in 20mm discretization length when compared to the other two discretization length. The difference in the cumulative gas flow between the discretization lengths 20mm and 10 mm are around 0.6 %. But the difference between 10mm and 15mm discretization length are just around 0.03%. So, it was evident that the readings between discretization length 10mm and 15mm are more accurate than the length 20mm. This is supported by the fact the readings of 10mm and 15 mm are comparable, which means the values are converging and accurate. If the model is simulated with 10mm it is marginally accurate and takes a little longer run time than the simulations when compared to 15mm. Therefore, a discretization length of 12mm was chosen which gives considerable accuracy and relatively shorter run time. All following experiments in this chapter is carried out with discretization length of 12 `mm to study the pulse in the rail

6.2.2 Gas rail pressure pulse analysis

The model was simulated with a tuned gas flow rate setting in such a way that the pre-chamber is completely scavenged at all engine speeds. The GR was tested in full pre-chamber scavenging condition as the maximum gas flow rate is required in this setting. So, the pressure pulse in the GR can be observed in the maximum flow rate condition. The tuned gas flow rate setting for different engine speed is given in the table 15.

Engine speed (RPM)	800	1200	1800	2200	2600
Gas flow rate (m^3/h)	0.149	0.291	0.640	0.764	1.07

Table 15 Tuned gas flow rate setting data for 100% scavenging

From the table 13, the maximum gas flow rate experienced by the GR is at engine speed of 2600 RPM. In case in the future the Volume of the pre-chamber is increased for research works, The GR will have to experience much more gas flow rate. So, the Model was simulated to observe the pressure pulse with a gas flow rate 2m^3/h which is twice the maximum gas flow rate the GR experienced in the previous simulation.

From the simulations, the pulse amplitude when the GR is operated at gas flow rate of 1 m^3/h and 2 m^3/h are 0.015 and 0.05 bar which are negligible. The figure 38 and 39 shows the pressure pulsations in the GR. The pre-chamber is completely scavenged with tuned gas flow rate setting for engine speed range of 1800-2000 RPM. But, regardless the tuning of gas flow, the scavenging did not go more than 75% at engine speeds above 2200 RPM.

This is because the maximum volumetric flow rate of the check valve connecting the gas rail and the pre-chamber was reached. From the figure 40 we can see that the for-check valve used, there is a cut-off in volumetric flow rate (circled) as that is maximum flow for the diameter (1.2mm). It is also evident that if the diameter of the check valve is increased to 1.5 mm, there is an increased volumetric flow through the check valve.

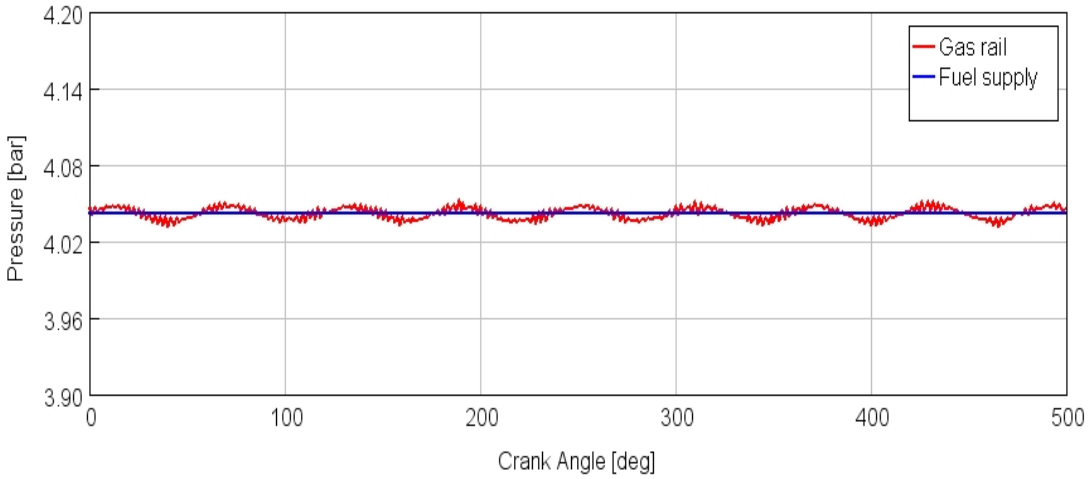

Figure 38 Pressure pulse in GR and fuel supply pressure to GR vs crank angle at 2600 RPM when gas flow rate is 1m^3/h

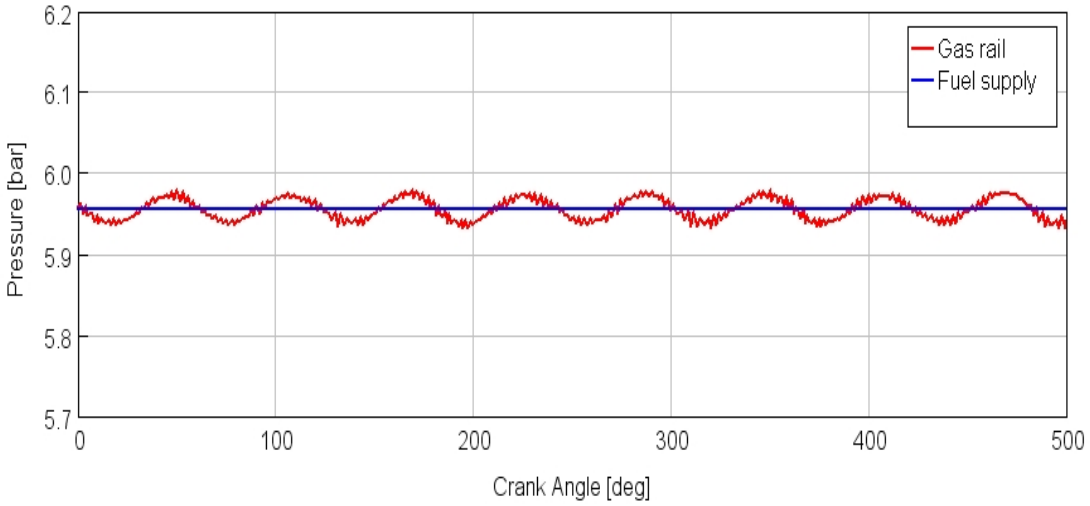

Figure 39 Pressure pulse in GR and fuel supply pressure to GR vs crank angle at 2600 RPM when gas flow rate is 2m^3/h

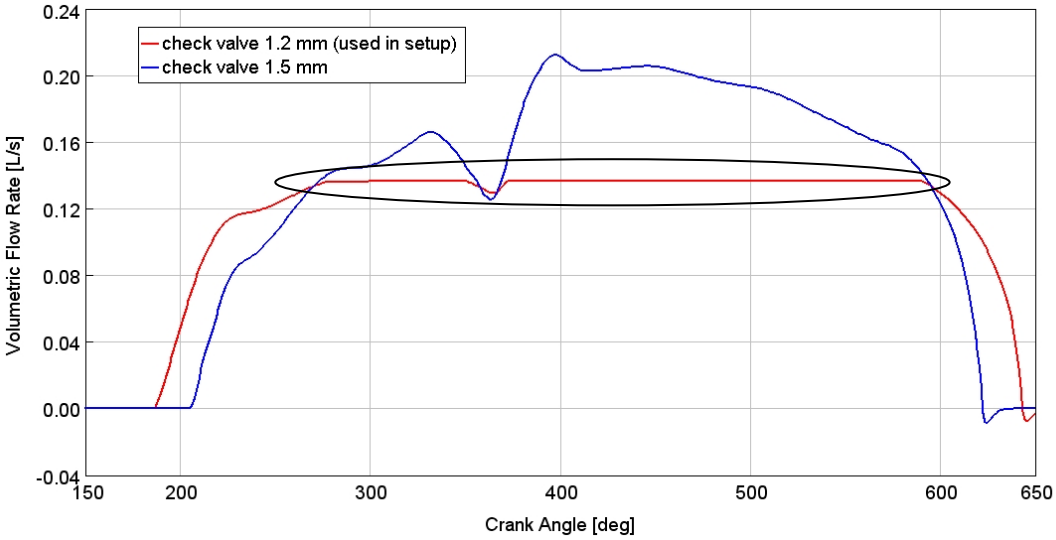

Figure 40 Volumetric flow rate through the check valve vs crank angle at 2600RPM with cut-off in volumetric flow rate circled

6.2.3 Gas rail dimension sensitivity analysis

The pulsation in the GR is the major factor which affects the chamber to chamber variation in cumulative gas flow. Even though the pulsations of the designed GR were negligible, it can be noticed that when the gas flow rate was increased from 1 m^3/h to 2 m^3/h, there was an increase in the pressure pulse amplitude in the GR. So, to make the GR compatible to extreme gas flow rate, the pulsation can be further reduced by changing the dimensions of the GR.

The lengths from the inlet for the GR to the outlet to the chambers, the plenum volume and the dimensions of the runner are the design parameters which has major impact on the chamber to chamber gas flow variations which are due to the pressure pulsations. The runner dimensions play a role in the change in the pulse formation as given by the equation (7) [11] given below. The runner dimensions can alter the frequency of the pulse formation and time it the pulse takes to reach the plenum area. This section aims in reducing the chamber to chamber cumulative gas flow variations by changing the dimensions of the runners and volume of the plenum area.

$$f_H = \frac{c}{2\pi}\sqrt{\frac{A}{lV}} \tag{7}$$

Where, f_H is the resonant frequency of the pressure pulse, ‘c’ is the speed of sound, ‘A’ is the cross-section area of the runner, ‘l’ is the runner length and ‘V’ is the plenum volume.

From the previous simulation it was known that the chamber to chamber cumulative gas flow variation at 2600RPM was 1.4 % The simulations were performed with gas flow rate of 1m^3/h and at engine speed of 2600 RPM. Different GR Dimensions were simulated. The runner length, runner diameter and plenum volume were changed in each simulation. The dimensions of the runner length, runner diameter and plenum volume were 50.8mm, 9.4mm and 119600mm^3 for the base GR designed.

From the simulation results, it is concluded that the change in the dimensions of GR doesn't have considerable reduction in the chamber to chamber cumulative gas flow variations. As the Base GR has already very low variations in the cumulative flow into the pre-chamber. The variations in the cumulative gas flow into the pre-chamber for different dimensional change in GR is shown in the figure 41. Increase of runner length or plenum volume decreases the chamber to chamber gas flow variations, whereas the increase of the runner diameter increased variations. The tested operating range of the GR with negligible pressure pulse is given below in table 16.

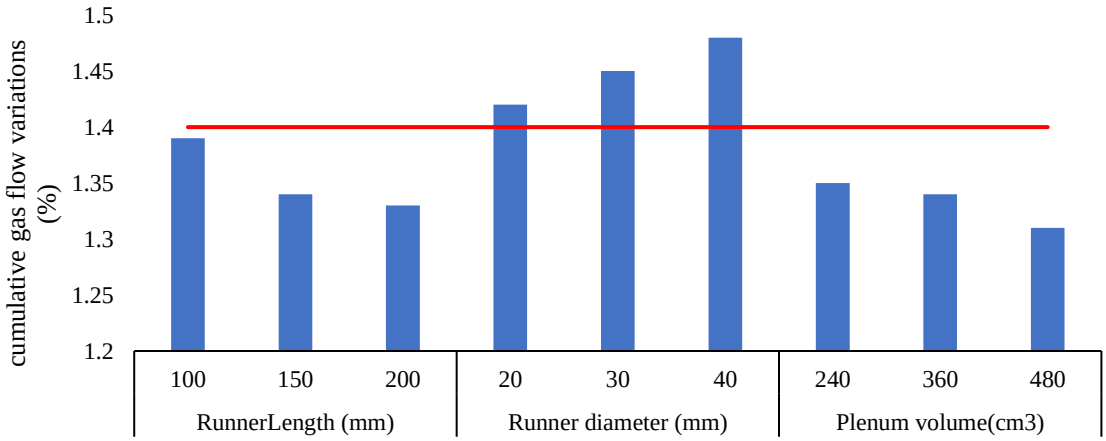

Figure 41 The variations in the cumulative gas flow into the pre-chamber for different dimensional change in GR with the variations in the Base GR marked in redline

Parameter	Range
Engine speed (RPM)	800 – 2600
Gas flow rate (m^3/h)	0 - 2
Throttle position (degree)	0 - 90
VGT rack position	0 - 1
EGR (%)	0 - 20

Table 16 Tested operating range of the GR with negligible pressure pulse

Summary and conclusion

Studies were conducted on the created 4-cylinder GT-POWER model. The existing model showed some contradictions when compared to the experimental setup. Hence, few improvements were made in the model to make it same as the experimental setup. The model was calibrated based on the experimental data. The full load torque curve of the model was calculated and compared with the original 4-cylinder SI engine. The performance map of the model was plotted for the 4-cylinder gas engine with pre-chamber.

The GR for the pre-chamber of a 4-cylinder gas engine were designed with the instrumentation fittings. The 3-D Model and manufacturing drawings of the GR was used to add GR design to the GT-power model. Simulations were performed to study effect of scavenging of pre-chamber in the model. Sensitivity analysis was performed on the GR dimensions to see how the performance of the GR changes.

Some key conclusions are given below:

- Both main and the pre-chambers are not considered closed by the GT-POWER. So, the specific combustion model given to the main and pre-chamber influence one another causing the variations in combustion timing and combustion duration.
- The CA50 of the GT-POWER model was swept from 15 to 30 degrees. There was an increasing trend in the torque output of the model till CA50-25 degree. The optimum CA50 for the 4-cylinder pre-chamber gas engine is 25 degrees.
- The EGR tuning is better than throttle angle tuning for controlling the exhaust temperature without drastically affecting the torque output of the engine.
- The 4-cylinder gas engine with pre-chamber gives a better torque output than the 4-cylinder SI original engine in the operating range.
- The lean operation limit of the 4-cylinder gas engine can be extended when the pre-chamber is scavenged.

- Pre-chamber scavenging reduces the thermal stress. High temperature may cause pre-ignition. Hence making the combustion unstable.
- the scavenged pre-chamber gives more ignition energy in the main chamber than the pre-chamber without the additional gas supply.
- Discretization length setting in model has an effect in cumulative gas flow data obtained from the simulations. The change of 10 mm in discretization length results in 0.6 % change in the cumulative gas flow values.
- The Model must have a tuned gas flow rate setting for each engine speed to achieve optimum cumulative gas flow into the pre-chamber for scavenging. There is low scavenging observed at engine speed above 2200 RPM even when the gas flow rate setting is tuned. This is due to the flow restriction of check valve with small diameter. This problem can be solved by replacing it with the check valve of diameter 1.5mm
- The pressure pulsations in the designed GR are negligible in the operating range of the engine. The GR rail has a maximum chamber to chamber cumulative gas flow variation of 1.4 % which occurs only at high engine speeds. Engine speeds below 2200 RPM has less than 1% change.
- The GR designed is the best possible design from the available instrumentation fittings. If the requirements demand a much lesser chamber to chamber cumulative gas flow variations, then a GR must be manufactured in house with an increased runner length or plenum volume.

Thesis contribution and suggestions

Contribution of this thesis:

- List of Components with Manufacturer name, model name and quantity to assemble a GR without pressure pulsation for a 4-cylinder scavenged pre-chamber gas engine
- 3-D model of the GR which can be used for CFD analysis of the GR if needed in the future.
- 4-cylinder GT-power model of the pre-chamber engine with required controller to perform the simulations with specific operating conditions.
- Tuned VGT rack position and EGR setting data which can be taken as reference to run experimental engine in the physical limits of the components in the experimental setup while developing a 4cylinder pre-chamber gas engine.
- Performance map of the 4-cylinder gas engine model with scavenged pre-chamber.
- Simulation data regarding the effect of pre-chamber scavenging percentage on the 4-cylinder gas engine model.
- Tuned gas flow rate setting data to get optimum scavenging in the pre-chamber for the engine operating range
- Designed GR operating range data which can be taken as a reference for future proceedings.
- Reference data of the dimensions sensitivity of the GR, which will be useful if a better performing GR must be manufactured in the future.

Future suggestions:

- The current experimentation has been performed with a check valve dimension of 1.2 mm. But, due to volumetric flow restrictions caused by the dimension, the diameter was arbitrarily changed to 1.5 mm, which yielded better results. But, the dimension needs to be checked with the industrial standard if present and the entire analysis must be done accordingly to that dimension.
- The experimentation can be carried out and verified with CFD analysis in any other software where chamber to chamber cumulative gas flow variations can be viewed easily and can be tuned and understood more in detail.
- The performance of the base GR has been studied and the changes in the dimension have been done to decrease the chamber to chamber cumulative gas flow variation. For future research and development, the effect of these changes in dimensions on the performance output of the engine can be carried out and studied to validate its effectiveness with regard to the engine performance.

References

[1] Available at: https://www.c2es.org/content/international-emissions/

[2] The Effect of Vehicular Emissions on Human Health *by Ronni Esther Rossman* Available at: http://teachers.yale.edu/curriculum/viewer/initiative_08.07.09_u

[3] Available at: https://www.afdc.energy.gov/fuels/natural_gas_basics.html

[4] Anne Prieur., Richard Tilagone., "*A Detailed Well to Wheel Analysis of CNG Compared to Diesel Oil and Gasoline for the French and the European Markets*'' SAE technical paper No. 2007-01-0037

[5] Toshiyuki Suga., Tadashi Muraishi., Thomas Brachmann., Fumio Yatabe., "*Potential of a Natural Gas Vehicle as EEV*" SAE technical paper No. 2000-01-186

[6] Vavra, J., Takats, M., Klir, V., and Skarohlid, M., "*Influence of Natural Gas Composition on Turbocharged Stoichiometric SI Engine Performance*," SAE Technical Paper 2012-01-1647, 2012, doi:10.4271/2012-01-1647.

[7] Li, G., et al.," Experimental *Study on the Ignition and Combustion Mechanisms of a Methane–Air Mixture in a Divided Constant-Volume Combustion Chamber. Energy & Fuels*", 2012. 26(8): p. 4696-4702.

[8] Vávra J, Syrovátka Z, Takáts M, Barrientos E. "*Scavenged Pre-Chamber on a Gas Engine for Light Duty Truck*." ASME 2016 Internal Combustion Engine Division Fall Technical Conference: V001T03A014. doi:10.1115/ICEF2016-9423.

[9] Heywood, J., B., "*Internal Combustion Engine Fundamentals*." New York: McGraw-Hill, 1988. Print.

[10] Baumgartner, L., Wohlgemuth, S., Zirngibl, S., and Wachtmeister, G., "*Investigation of a Methane Scavenged Pre-chamber for Increased Efficiency of a Lean-Burn Natural Gas Engine for Automotive Applications*," *SAE Int. J. Engines* 8(2):921-933, 2015, doi:10.4271/2015-01-0866.

[11] Ricardo, H.R., *Internal-combustion engine*. 1918, Google Patents.

[12] Zbynek Syrovatka, Michal Takats, and Jiri Vavra "*Analysis of Scavenged Pre-Chamber for Light Duty Truck Gas Engine*" SAE Technical Paper 2017-24-0095, 2017, doi:10.4271/2017-24-0095.

[13] GT-Suite manual

[14] Yeliana, C. Cooney, J. Worm, D. Michalek, J. Naber "*WIEBE FUNCTION PARAMETER DETERMINATION FOR MASS FRACTION BURN CALCULATION IN AN ETHANOL-GASOLINE FUELLED SI ENGINE*" *Journal of KONES Powertrain and Transport, Vol. 15, No. 3 2008*

[15] Ashish Shah 'Improving the Efficiency of Gas Engines using Pre-chamber Ignition' Lund University

[16] Available at: http://petrolsmell.com/2012/07/01/emissions-control-in-cylinder/

[17] Siti Khalijah Mazlan "*Study of Direct Injection and Pre-Chamber Application in Light Duty Gaseous Fuel Engines*" School of Engineering, College of Science Engineering and Health, RMIT University

[18] ANDERS N. JOHANSSON "*Challenges and Advantages of Stratified Combustion in Gasoline Direct-Injected Engines*" Department of Applied Mechanics, Chalmers University of technology.

[19] Available at: https://www.dieselnet.com/tech/air_turbo_vgt.php

[20] Available at: http://faq.outclub.ru/download/pajero_iv/maintenance/Service_Manual_2008_2013/2013/15/html/M215000900040200ENG.HTM

[21] ŠŤOURAL, Martin. DP 2014 - SM06: Zapalovací komůrka pro plynový motors nepřímým zážehem. Praha 2014. Diplomová práce. ČVUT v Praze. Vedoucí práce Ing. Jiří Vávra, PhD.

[22] Amit Kumar Gupta Abhishek Mishra "*Design and Development of Inlet Manifold for Six Cylinder Engine for Truck Application*" ISSN - 2250-1991 https://www.researchgate.net/publication/274925435_Design_and_Development_of_Inlet_Manifold_for_Six_Cylinder_Engine_for_Truck_Application

[23] United States Patent number: US8324792B2
Available at: https://patents.google.com/patent/US8324792

[24] United States Patent number: US8857405B2
Available at : https://patents.google.com/patent/US8857405

[25] Fraser-N. Parsons P. Attard, W. and E. Toulson. A turbulent jet ignition pre-chamber combustion system for large fuel economy improvements in a modern vehicle powertrain. SAE Int. J. Engines 3(2):20-37, 2010. doi:10.4271/2010-01-1457

[26] Velders GJM., "*Effect of greenhouse gas emissions on stratospheric ozone depletion*" Report 722201011, Netherlands National Institute for Public Health and the Environment RIVM.

[27] Moriarty, Patrick & Honnery, Damon. (2016). *Global Transport Energy Consumption*. 10.1002/9781119066354.ch61.

[28] Available at : https://ec.europa.eu/transport/sites/transport/files/2017-01-fuel-price-comparison.pdf

[29] Hugh Blaxill, Michael Bunce, "*The Development of a Pre-Chamber Combustion System for Lean Combustion of Liquid and Gaseous Fuels* "MAHLE Powertrain LLC, Farmington Hills, MI, USA

[30] Elisa Toulson, Andrew Huisjen, Xuefei Chen, Guoming Zhu and Harold Schock "Spark Ignition and Pre-Chamber Turbulent Jet Ignition Combustion Visualization" SAE 2012-01-0823

[31] Koji Yamanaka, Yosuke Shiraga, and Shunsaku Nakai "Development of Pre-chamber Sparkplug for Gas Engine" JSAE 20119147 SAE 2011-01-1870

List of figures

List of tables

List of Files in attached CD

1. Thesis.Pdf
2. 4CYLINDER SCAVENGED PRE-CHAMBER.gtm
3. Rail_draft.pdf
4. CAD Model
    4.1. Hex_nipple.prt
    4.2. Male_adapter.prt
    4.3. Pressure_sensor.prt
    4.4. Relief_valve.prt
    4.5. Tee.prt
    4.6. Rail.asm

Attachments

Attachment A

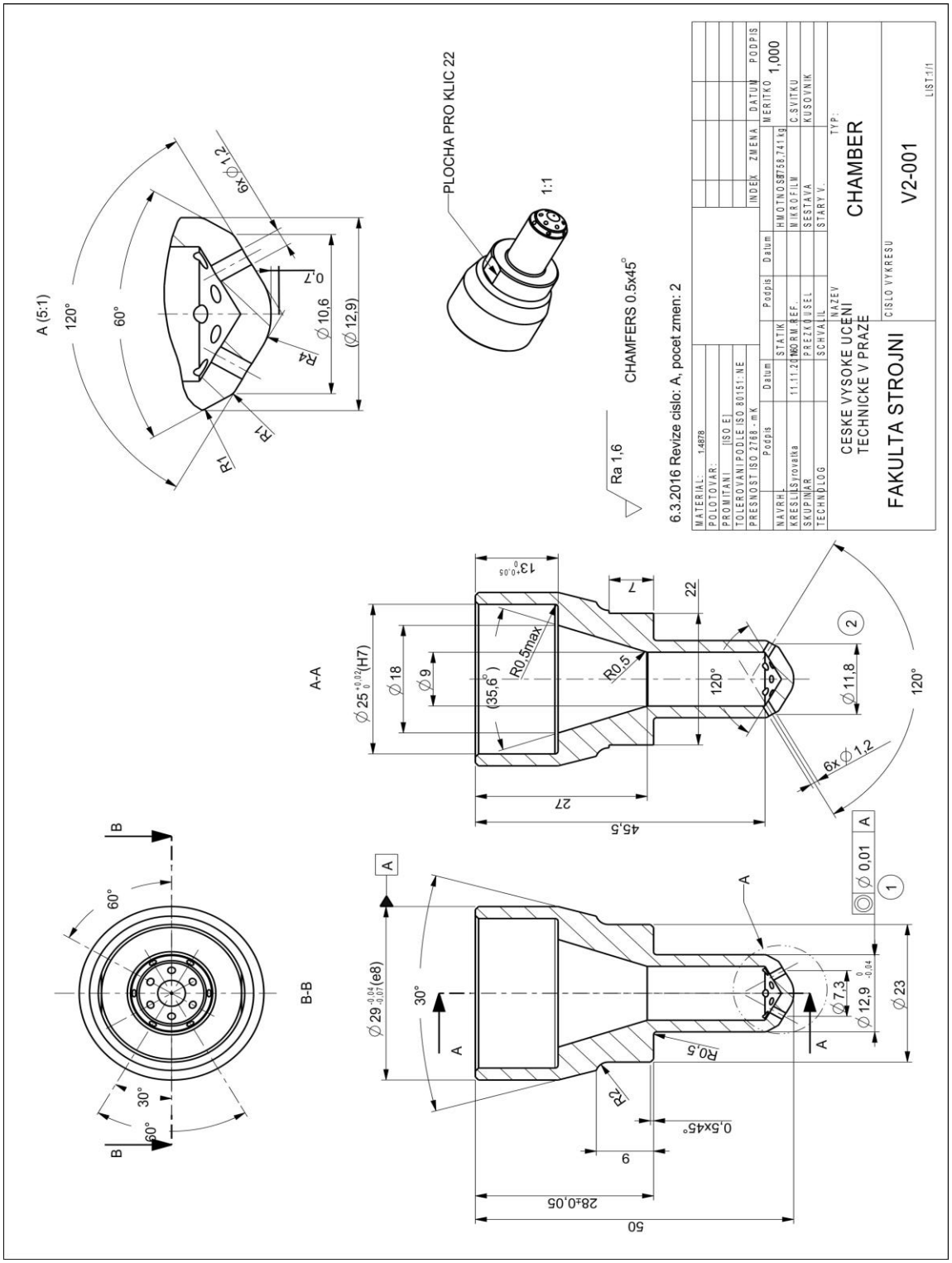

Attachment B

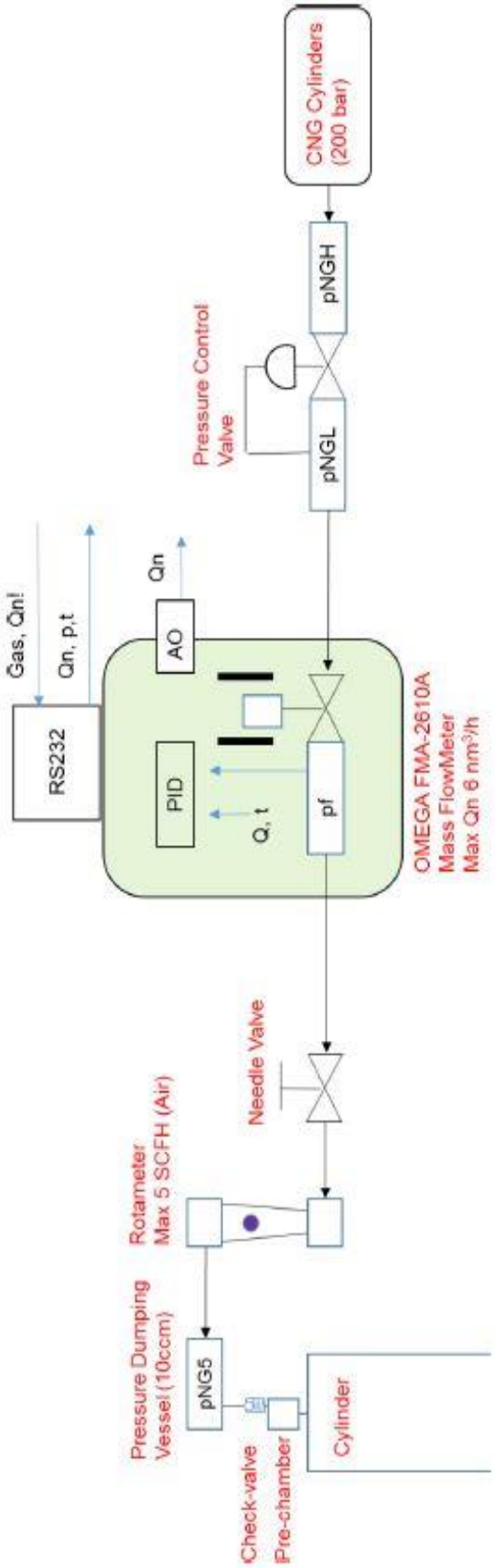

Attachment C

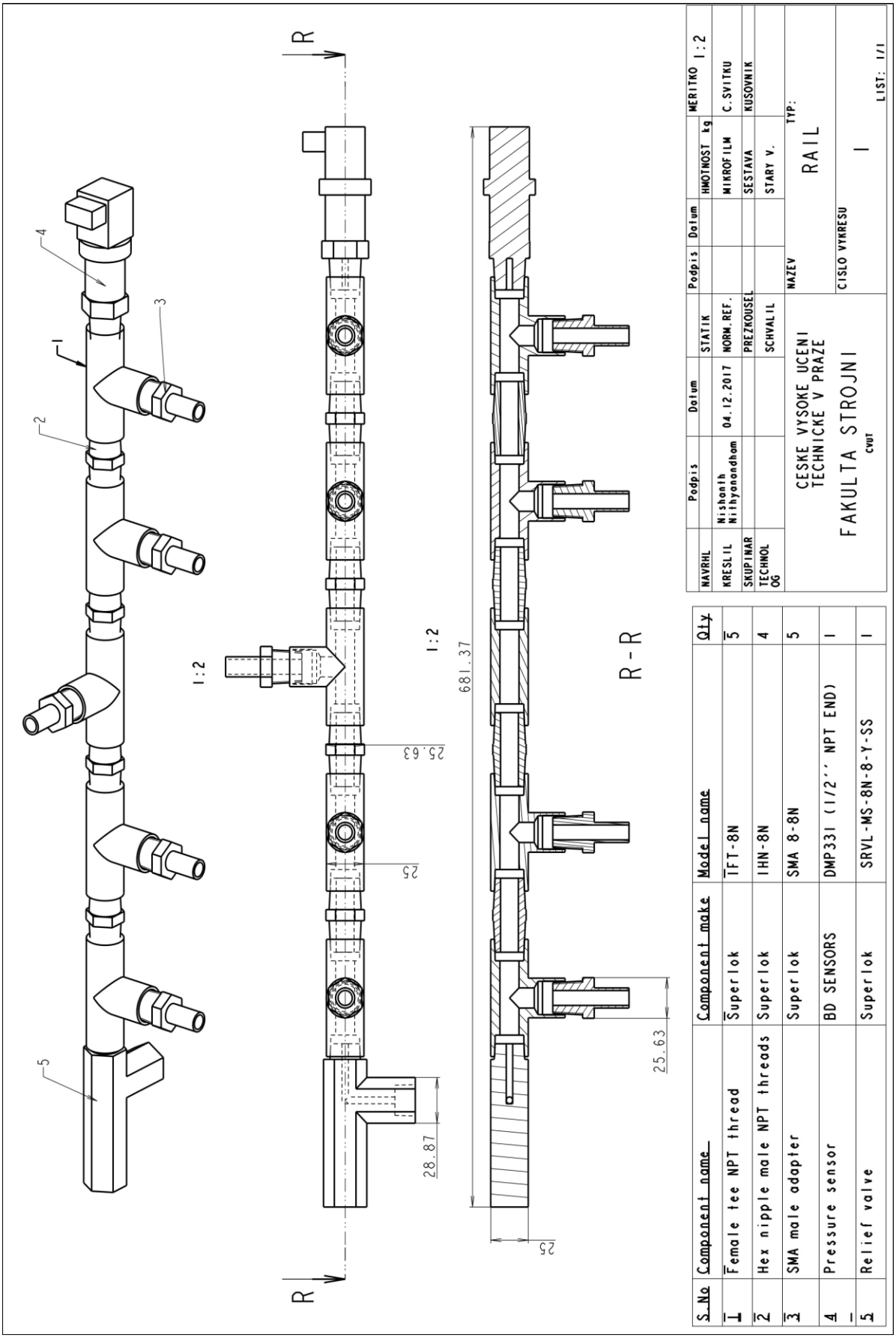

S.No	Component name	Component make	Model name	Qty
1	Female tee NPT thread	Superlok	TFT-8N	5
2	Hex nipple male NPT threads	Superlok	IHN-8N	4
3	SMA male adapter	Superlok	SMA 8-8N	5
4	Pressure sensor	BD SENSORS	DMP331 (1/2'' NPT END)	1
5	Relief valve	Superlok	SRVL-MS-8N-8-Y-SS	1

	Podpis	Datum		Podpis	Datum		
NAVRHL			STATIK			HMOTNOST kg	MERITKO 1:2
KRESLIL	Nishanth Nithyanandham	04.12.2017	NORM. REF.			MIKROFILM	C.SVITKU
SKUPINAR			PREZKOUSEL			SESTAVA	KUSOVNIK
TECHNOLOG			SCHVALIL			STARY v.	

CESKE VYSOKE UCENI TECHNICKE V PRAZE
FAKULTA STROJNI
CVUT

NAZEV: RAIL
TYP:
CISLO VYKRESU: 1
LIST: 1/1

Attachment D

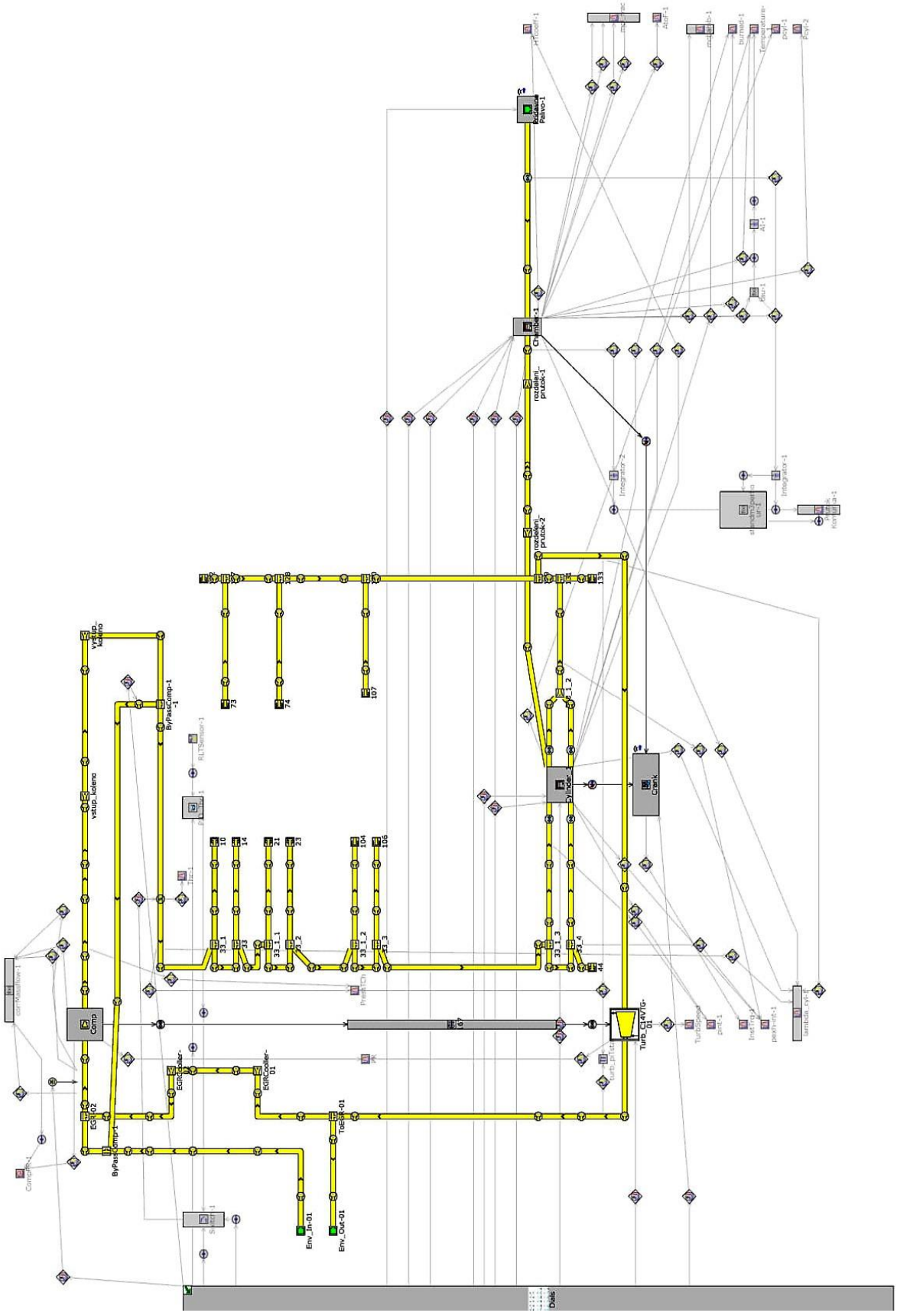

Attachment E